ABSTRACT

Title of dissertation: MODELING THE TRANSFER OF DRUG RESISTANCE IN SOLID TUMORS

Matthew Harrington Becker
Doctor of Philosophy, 2018

Dissertation directed by: Dr. Doron Levy
Department of Mathematics

ABC efflux transporters are a key factor leading to multidrug resistance in cancer. Overexpression of these transporters significantly decreases the efficacy of anti-cancer drugs. Along with selection and induction, drug resistance may be transferred between cells, which is the focus of this dissertaion. Specifically, we consider the intercellular transfer of P-glycoprotein (P-gp), a well-known ABC transporter that was shown to confer resistance to many common chemotherapeutic drugs.

In a recent paper, Durán *et al.* studied the dynamics of mixed cultures of resistant and sensitive NCI-H460 (human non-small cell lung cancer) cell lines [1]. As expected, the experimental data showed a gradual increase in the percentage of resistance cells and a decrease in the percentage of sensitive cells. The experimental work was accompanied with a mathematical model that assumed P-gp transfer from resistant cells to sensitive cells, rendering them temporarily resistant. The mathematical model provided a reasonable fit to the experimental data.

In this dissertation we develop three new mathematical model for the transfer

of drug resistance between cancer cells. Our first model is based on incorporating a resistance phenotype into a model of cancer growth [2]. The resulting model for P-gp transfer, written as a system of integro-differential equations, follows the dynamics of proliferating, quiescent, and apoptotic cells, with a varying resistance phenotype. We show that this model provides a good match to the dynamics of the experimental data of [1]. The mathematical model further suggests that resistant cancer cells have a slower division rate than the sensitive cells.

Our second model is a reaction-diffusion model with sensitive, resistant, and temporarily resistant cancer cells occupying a 2-dimensional space. We use this model as another extension of [1]. We show that this model, with competition and diffusion in space, provides an even better fit to the experimental data [1]. We incorporate a cytotoxic drug and study the effects of varying treatment protocols on the size and makeup of the tumor. We show that constant infusion leads to a small but highly resistant tumor, while small doses do not do enough to control the overall growth of the tumor.

Our final model extends [3], an integro-differential equation with resistance modeled as a continuous variable and a Boltzmann type integral describing the transfer of P-gp expression. We again extend the model into a 2-dimensional spatial domain and incorporate competition inhibited growth. The resulting model, written as a single partial differential equation, shows that over time the resistance transfer leads to a uniform distribution of resistance levels, which is consisten with the results of [3]. We include a cytotoxic agent and determine that, as with our second model, it alone cannot successfully eradicate the tumor. We briefly present a second extension

wherein we include two distinct transfer rules. We show that there is no qualitative difference between the single transfer rule and the two-transfer rule model.

MODELING THE TRANSFER OF DRUG RESISTANCE IN SOLID TUMORS

by

Matthew Harrington Becker

Dissertation submitted to the Faculty of the Graduate School of the
University of Maryland, College Park in partial fulfillment
of the requirements for the degree of
Doctor of Philosophy
2018

Advisory Committee:
Professor Doron Levy, Chair/Advisor
Professor Pierre-Emmanuel Jabin
Professor Antoine Mellet
Professor Maria Cameron
Professor Sergei Sukharev

Dedication

For my wife, Sarah.

Thank you for always being by my side.

Acknowledgments

First and foremost I wish to thank my advisor, Dr. Doron Levy for this incredible chance to learn from him and work in the field of mathematical oncology. He was the reason I first heard about the University of Maryland AMSC graduate program as an undergraduate and I'm eternally grateful for the opportunity to work and collaborate with him.

I'd also like to thank several other professors for their help, wisdom, and encouragement. Thanks to Dr. Pierre-Emmanuel Jabin and Dr. Wolfgang Losert for having been with me since my oral preliminary exam. Thank you to Dr. Antoine Mellet for the invaluable help in the analysis of our reaction-diffusion model. Special thanks also to Dr. Maria Cameron and Dr. Sergei Sukharev for agreeing to be part of my committee.

A couple of my, now graduated, fellow graduate students have been instrumental in guiding me through this journey. I want to thank Jim Greene and Geoff Clapp for their technical expertise as well as their constant willingness to impart advice. Thanks to both of you for setting such an example for me to follow. Thanks to Kilian Cooley for your help with my finite difference codes, and to Cara Peters for countless conversations over the last years. Thanks also to Ryan Kirk, Matt Whiteway, Oliver Lum, Asia Wyatt, Zsolt Payor-Gyulai, Colleen Stock, and so many more for all of the discussions about math and otherwise and for making graduate school such a memorable experience.

Thanks especially to my twin brother, Tim. We've spent the last 20 years talk-

ing mathematics and I have no idea what it would be like without the interminable list of memories, experiences, and shared knowledge.

Thank you to the rest of my family: Mom, Dad, and Trudy. Mom and Dad, you've set the best example I could ever ask for in academia and maybe someday I'll have students of my own who talk about me in the ways all your students do of you. Trudy, thanks for being the smartest kid in the family. Your ability to excel in everything has pushed me to continue to work as hard as possible, if only to just once beat you in something!

Finally, thank you again to my wife Sarah. You were there when I got accepted into this program, when I decided to come, and at every important step along the way, especially the most important step when we got married two and half years ago. With the amount of times we've talked through every bit of struggle or joy of advancement, there is no person who has contributed more to this than you. I'm eternally grateful that I get to spend my life with you and I thank you for every minute of it.

Contents

List of Tables

List of Figures

Chapter 1: Introduction

The work in this dissertation uses mathematical models to study the transfer of a specific protein, P-glycoprotein, between cells and how this transfer affects multidrug resistance in cancer. Since this work integrates mathematics and cancer biology, we begin with a discussion of the biology in our models. This opening chapter will give a brief primer of the mechanisms of cancer.

1.1 Biology of Cancer

Cancer is a worldwide public health issue and the second leading cause of death in the United States [4]. In the United States alone, there were an estimated 1.5 million new cases in 2016, with almost 600,000 expected deaths [4]. The lifetime probability of being diagnosed with some type of invasive cancer hovers around 40%, with that number slightly higher for men and slightly lower for women [4]. Cancer is a group of diseases arising from the loss of control of cell growth [5]. Uninhibited cellular growth is the most prevalent marker of cancer. Malfunctions in the systems that regulate this growth can happen anywhere in the body. This explains the many different types of cancers, from blood cancers including leukemias to solid tumors including the most common- breast, lung, and prostrate cancers [4].

In order to achieve unlimited growth, apoptosis must be at least partially inhibited [6,7]. Apoptosis is the inherent mechanism used in cellular self-destruction [8]. Cancer occurs when a series of mutations in the proteins constructing cellular growth control systems cause the loss of appropriate functionality [5]. These mutations can be genetic, occuring during the copying of DNA, as well as epigenetic, induced by outside factors or events [5,9]. Common carcinogens, such as smoking, radioactive materials, and sunburns, are activities and events that can damage DNA and cause mutations [5,10,11]. The uninhibited growth can eventually disrupt organ function, leading to death [12]. Interestingly, since many cancers develop after child-bearing years, there is no evolutionary pressure to limit these mutations [5].

With the improvement in treatment protocols and therapies, several cancers have high 5-year survival rates if diagnosed early. For example, the average 5-year survival rate for breast cancer is 90% [13]. Once cancerous cells have metastasized and a secondary tumor begins growing elsewhere, the 5-year survival rate plummets. If a breast tumor has undergone metastasis, the 5-year survival rate drops to 26% [13]. Cancer cells are also able to vascularize through angiogenesis, the process of creating their own blood vessels to sustain large tumors [14,15].

Surgery, chemotherapy, radiotherapy, and immunotherapy are currently the four main protocols for treatment. Some form of surgery has been prevalent since the time of the ancient Greeks, where Hippocrates first identified a tumor as a *karkinos* [16]. Surgical removal of a solid tumor is still the most common method but it is now known that surgery alone might not deliver a cure. There may be cancer cells that are not removed through surgery and are able to regrow the tumor,

so chemotherapy and radiotherapy is used as an adjuvant therapy. If a tumor is too large or not sufficiently isolated, chemotherapy may be used first as neoadjuvant therapy to shrink the tumor to a manageable size for surgery [17].

Chemotherapy is the delivery of a poisonous chemical compound used to target cells. Most drugs slow down or stop mitosis [18–20]. While this is the most straightforward way of decreasing the tumor load, it often cannot eradicate the tumor completely. The main reason for treatment failure is due to the development of drug resistance, wherein cancer cells evolve to become less affected by the chemotherapeutic agent [21]. Radiation therapy, or radiotherapy, damages the cancer cell DNA through ionizing radiation, leading to apoptosis [22, 23]. Immunotherapy prods the immune system, either directly or indirectly, to attack and suppress tumor growth [24, 25]. The immune response may act by slowing down the proliferation and growth of cancer cells [25]. Consequently, immunotherapy does not yield drug resistance in the way that chemotherapy does [26]. There are now well over 100 chemotherapeutic agents that can be used in combinations and alongside immunotherapies.

In all cases, drugs target the cell cycle. Cells in quiescence are not affected until they enter an active proliferation stage. Most therapies do not differentiate between cancerous and healthy cells. They are adjusted to the rate of proliferation of cancer cells, which is why fast proliferating cells such as hair cells are adversely affected by cancer treatments [27]. There is a balance between doses that are enough to affect the tumor and not too high to cause substantial damage to healthy tissues.

1.2 Drug Resistance

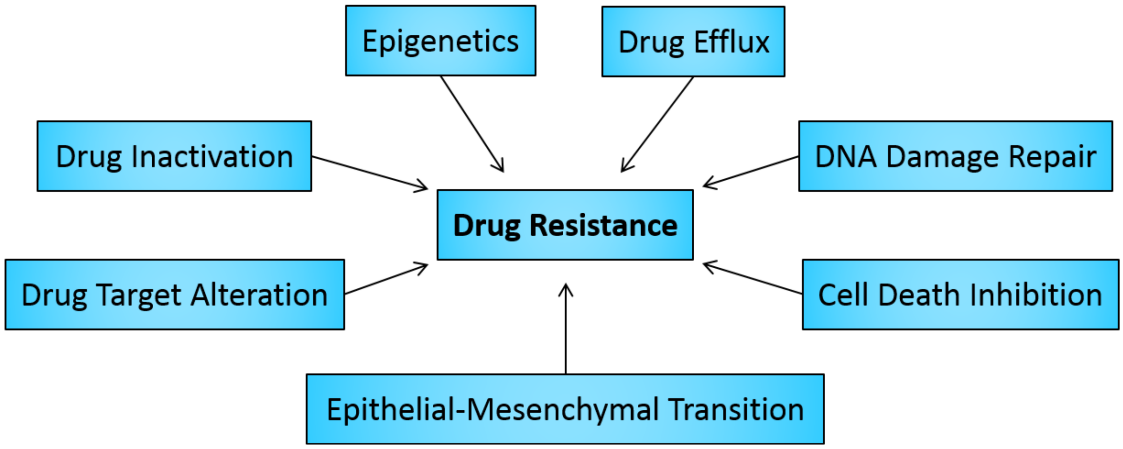

Figure 1.1: The most prevalent mechanisms by which a cancer cell inherits and exhibits drug resistance. Figure adapted from [28].

Resistance of tumor cells to anti-cancer drugs is one of the most important challenges facing oncologists. The Norton-Simon hypothesis states that the reduction in tumor volume resulting from chemotherapy is proportional to the unperturbed rate of growth of a tumor of the same size [29, 30]. Unfortunately drug resistance can slow down this reduction. Drug resistance can be caused by intrinsic factors, such as location in the tumor, or by genetic events such as mutations [31]. Multidrug resistance has been previously explained as an overexpression of ABCB1 but there are a plethora of other mechanisms at play as well, including decreased drug uptake and evasion of apoptosis [31]. As drugs are administered, cancer cells can mutate and their progeny become more resistant and the drugs less effective [32]. Understanding the mechanisms that cause and propagate resistance is paramount to devising methods for overcoming it.

When administering drugs to cancer patients there are two main types of drugs: (i) cytostatic drugs, which target cancer cells by slowing down their proliferation rate and (ii) cytotoxic drugs, which kill the cells. Both cytostatic and cytotoxic drugs can harm healthy cells yet have an increased effect on tumor cells, although there are cytostatic drugs that act on the tumor environment which can avoid uneccessary harm to healthy cells [33]. Not all cancer cells exhibit the same traits, genotypically or phenotypically, and so tumor heterogeneity is very important in understanding the effects of both types of drugs. This dissertation will focus on one specific protein overexpression that causes resistance to multiple drugs simultaneously.

Antineoplastic resistance is often the key impediment to effective cancer treatment. Though advances in early detection have increased survival rates across several cancer subtypes, resistance to chemotherapy is prevalent [34, 35], and the majority of patients will relapse at a certain point following treatment. Therapeutic failure may be attributed to intrinsic tumor heterogeneity prior to therapy (e.g., spatial localization of cancer cells within a tumor, initial cellular genetic landscape, cell-cycle length variations, etc.) or induced tumor heterogeneity after initiation of therapy, such as altered molecular signaling, genetic modification, and microenvironmental alterations.

Development of resistance to one drug can also lead to resistance to other structurally and mechanistically unrelated drugs, a phenomenon referred to as multidrug resistance (MDR). MDR can be understood through different biological factors and is often identified with drug efflux [36]. There has been increasing evidence that drug cellular uptake is regulated by transport proteins expressed on the cellular

membrane, which are responsible for drug transport across the plasma membrane and throughout the cell. One such example is the family of ABC (ATP Binding Cassette) transporters. ABC transporters can pump away chemotherapeutic agents, which allow certain cells to withstand the drugs' cytotoxic effect [31]. These non drug-specific transporters provide a mechanism for the cells to resist unrelated drugs, which then leads to a chemotherapy breakdown. While ABC transporters have important roles in the importation of nutrients and exportation of toxic molecules [37], their overexpression is a serious obstacle in anti-cancer therapies.

1.2.1 P-glycoprotein

P-glycoprotein (P-gp), a product of the ABCB1 (*mdr1*) gene, is a well-known ABC transporter that correlates with MDR [38, 39]. It has been shown to confer resistance to many common chemotherapeutic drugs [40–43] and is expressed in many human cancers [44]. In normal human tissues it is concentrated in cells in the liver, pancreas, kidney, colon, and jejunum [45]. P-gp targets xenobiotics and there is a lengthy list of substrates it can expel, including common anti-cancer drugs doxorubicin, paclitaxel, and imatinib. The MDR1 gene encodes the transmembrane P-gp pump that cells use to excrete structurally and chemically diverse drugs [8]. A drug molecule is bound by the P-gp's cytoplasmic domain; the protein subsequently uses ATP hydrolysis and opens itself to the extracellular space and expels the drug molecule [8]. The overexpression of P-gp can lead to resistance of more than 100 times higher than normal cells [46]. Two studies in 2005 showed resistant

populations can spread their resistance to sensitive cells [47, 48]. More recently, intracellular membrane nanotubes were shown to carry P-gp between neighboring cells [44].

Drug resistance is often a multifactorial, complex process that arises through a series of genetic and non-genetic changes across multiple cancers. Such changes can be the consequence of drug administration (therapy-dependent), or can be acquired independently of any drug (therapy-independent). The focus of this work is on drug resistance that may be transferred between cells, e.g., via cell-to-cell communication.

1.3 Setup of the Dissertation

In this dissertation we develop new mathematical models for the transfer of drug resistance between cancer cells. Our first model, studied in Chapter 3, is based on incorporating a resistance phenotype into a model of cancer growth [2]. The resulting model for P-gp transfer, written as a system of integro-differential equations, follows the dynamics of proliferating, quiescent, and apoptotic cells, with a varying resistance phenotype. We show that this model provides a good match to the dynamics of the experimental data of [1]. The mathematical model further suggests that resistant cancer cells have a slower division rate than the sensitive cells.

The second model, studied in Chapter 4, is a set of reaction-diffusion equations governing the growth of sensitive and resistant cancer cells in the presence of a chemotherapeutic agent. Since the resistant cells in the experiments from [1] were

induced through doses of doxorubicin, that is the drug we consider here. We allow the drug efflux action of the P-gp pumps to affect the diffusion of the drug and incorporate a temporarily resistant phenotype. We study the effects of constant infusion versus on/off treatment of the drug. We show the lack of existence of an optimal therapy under the constraints of the model.

Our third model, studied in Chapter 5, continues the work of [3,49] in studying a set of Boltzmann type integro differential equations to investigate resistance as a continuous variable. We extend this measure by including two spatial dimensions and density-dependent proliferation. The resulting reaction-diffusion equation incorporates the reaction as an integral term summing over all the of nearby transfers of resistance that result in a specific resistance level. We show that the model agrees with the findings of [3]. The model is then extended by incorporating the effects of the cytotoxic drug doxorubicin. We study different protocols and demonstrate that there is no optimal way to control the propagation of resistance.

Chapter 2: Mathematical Models of Multidrug Resistance

Early mathematical models of drug resistance in cancer are due to Goldie & Coldman [50]. Their work is based on a probabilistic model in which the presence of a drug leads to cellular mutations which results in drug resistance. The approach of Goldie & Coldman was not immediately widely accepted. Rosen [51] believed that resistance was independent of dose and proposed a model for cellular competition, arguing that resistance is selected through competition and is not induced by the drug, as Goldie & Coldman had argued. To emphasize his point, Rosen used for [51] the same title used by Goldie & Coldman a year earlier. It has been shown since that selection and induction can coexist and both lead to drug resistance [52–55]. In this section we provide details about some of the models that were developed to describe MDR.

2.1 Recent Models

Panetta [56] developed a heterogeneous tumor model with induced resistance:

$$\frac{dx}{dt} = [r_1 - d_1(t)]x, \tag{2.1a}$$

$$\frac{dy}{dt} = b_1 d_1(t)x + [r_2 - d_2(t)]y. \tag{2.1b}$$

In this model $x(t)$ represents sensitive cell mass and $y(t)$ represents resistant cell mass. b_1 represents the resistant cell induction rate due to the effects of the chemotherapy drug d_1. A second function of time, d_2, represents the effect of the drug on resistant cells, so $d_2 \equiv 0$ if they are completely resistant. Both sets of cells exhibit exponential growth. Panetta used this model to study treatment protocols and find at what point the tumor stops regressing with the drug.

Jackson & Byrne [14] added a spatial component through a radially symmetric reaction-diffusion model without induction from the drug:

$$\frac{\partial d}{\partial t} + \nabla \cdot (\mathbf{u}d) = \nabla \cdot (D(r)\nabla d) + \Gamma(r)(d_b(t) - d) - \lambda d, \tag{2.2a}$$

$$\frac{\partial p}{\partial t} + \nabla \cdot (\mathbf{u}p) = D_p \Delta p + F_p(p) - C_p(d, p), \tag{2.2b}$$

$$\frac{\partial q}{\partial t} + \nabla \cdot (\mathbf{u}q) = D_q \Delta q + F_q(q) - C_q(d, q). \tag{2.2c}$$

This model includes an equation for the drug, $d(t)$, with diffusion term $D(r)$ assuming that the distance from the center of the tumor may affect diffusion. $\Gamma(r)$ is

the rate coefficient of blood-tissue transfer and $d_b(t)$ is the prescribed drug concentration in the vasculature. $p(t)$ represents the sensitive cells and $q(t)$ the resistant cells. F_p and F_q are proliferation rates and the terms C_p and C_q are the effect of chemotherapy. Jackson & Byrne showed that the effectiveness of the treatment protocols depended on the initial make-ups of the tumor.

MDR has been studied in connection with tumor heterogeneity [14, 57–59]. Lorz *et al.* [59] modeled resistance as a continuous variable and demonstrated that the presence of a cytotoxic agent leads to diminished heterogeneity and a population of overwhelmingly resistant cells. Lavi *et al.* extended the approach of Lorz to model intratumoral heterogeneity [57]. For a further review on mathematical models of MDR we refer to [58] and the references therein.

2.2 Optimal Treatment

Mathematical tools can be used to identify treatment strategies that optimize certain aspects, such as minimizing the overall tumor load or minimizing the amount of drug.

Panetta [56] studied a sequential drug administration and used the ratio of resistant to sensitive cells to analytically show when to switch from one drug to another. Goldie & Coldman [60] attempted to determine whether sequential or combination therapies are more effective. While combination therapy may be impractical due to high toxicity, they determined that it is the optimal option. Lorz *et al.* [59] found a specific parameter set for which resistance will occur based on the

amount of drug dose, and then in [61] studied a combination of cytotoxic and cytostatic drugs. They showed intra-tumor heterogeneity is decreased under constant infusion of a cytotoxic drug, with drug resistance levels rising dramatically.

In the early 2000s De Pillis & Radunskaya studied optimal control within models of cancer treatment [62–64]. They emphasize the role of the immune system in mediating the growth of the tumor. Their model from [63] is written as:

$$\frac{dN}{dt} = r_2 N(1 - b_2 N) - c_4 TN - a_3(1 - e^{-u})N, \tag{2.3a}$$

$$\frac{dT}{dt} = r_1 T(1 - b_1 T) - c_2 IT - c_3 TN - a_2(1 - e^{-u})T, \tag{2.3b}$$

$$\frac{dI}{dt} = s + \frac{\rho IT}{\alpha + T} - c_1 IT - d_1 I - a_1(1 - e^{-u})I, \tag{2.3c}$$

$$\frac{du}{dt} = v(t) - d_2 u. \tag{2.3d}$$

N(t) is the number of normal cells, T(t) the tumor cells, I(t) the immune cells, and u(t) the drug. There is competition between the normal cells and tumor cells. Interaction between the immune cells and the tumor cells can lead to inactivation of immune cells but also can lead to the death of the tumor cells. The presence of tumor cells stimulates the immune response so immune cells exhibit nonlinear growth when interacting with tumor cells. Finally, all the cells are affected by the existence of the drug u with a fractional cell kill term. They show that the optimal drug treatment protocol is 'bang-bang', where either a full dose or zero dose is given for each time step.

In the last 10-15 years Ledzewicz & Schättler have been developing optimal

control theory and its application to anti-cancer therapies. In [65] they consider an ODE model with sensitive compartment $S(t)$ and resistant compartment $R(t)$:

$$\frac{dS}{dt} = -aS + (2-q)aS + rcR, \tag{2.4a}$$
$$\frac{dR}{dt} = -cR + (2-r)cR + qaS. \tag{2.4b}$$

The first terms on the right are the deaths of the mother cells. The second terms include the progeny along with the return mutations back from resistant to sensitive (and vice versa). Inclusion of a constant drug dose u changes the representation to be as follows:

$$\frac{dS}{dt} = -aS + (1-u)(2-q)aS + rcR, \tag{2.5a}$$
$$\frac{dR}{dt} = -cR + (2-r)cR + (1-u)qaS. \tag{2.5b}$$

As in general optimal control problems, the problem is formulated as to optimize an objective functional,

$$J = \int_0^T L(N,u)dt + \phi(T, N(T)). \tag{2.6}$$

In any model the necessary conditions, including minimum and transversality conditions, for the existence of an optimal control are given by the Pontryagin Maximum

Principle [66, 67]. For the type of functionals 2.6, Ledzewicz & Schättler show the existence of optimal solutions and conditions for singular controls. For more detail we refer to their books [67, 68].

2.3 P-Glycoprotein

Several mathematical models for specific mechanisms of resistance have been derived and studied. As mentioned in 1.2.1, P-glycoprotein is one of the most well-known of these mechanisms. It is an ABC transporter than allows cells to excrete a variety of anti-cancer drugs. Michelson and Slate [69] derived a model incorporating adenosine triphosphate (ATP) and adenosine biphosphate (ADP). They note that the efflux generated by Pgp overexpression is only possible when ATP is also present since it needs to bond with p170. A later work [70] includes the presence of an inhibitor. A biophysical model was introduced by Panagiotopoulou *et. al* [71]. They show that the internal makeup of the tumor and the interaction between the drug molecular weight and the membrane are drivers of MDR. These factors impact the chance of an interaction between the drug drug and a protein transporter.

Relatively little attention has been given in the mathematical community to modeling the transfer of drug resistance between cells. A recent work by Durán *et al.* [1], derived two models for P-gp transfer assuming P-gp expression has a discrete characteristic: P-gp in a cell is either overexpressed or not. These models are written as a coupled system of ordinary differential equations (ODEs) describing the behavior of sensitive cells (S), resistant cells (R), and temporarily resistant cells

(S_R). Interaction between sensitive and resistant cells allows the resistant population to transfer P-gp to the sensitive cells, which become temporarily resistant. Since this is a phenotypic change, the progenies of these cells revert back to a sensitive state. The resistant cells are not affected by the interaction and exhibit logistic growth. The first model, with no consideration of the action of a drug, of [1] is given by

$$\frac{dS}{dt} = \frac{S}{\tau_s}\left(1 - \frac{R+S+S_R}{K}\right) - \frac{SR}{\tau_c} + \frac{S_R}{\tau_*}, \tag{2.7a}$$

$$\frac{dR}{dt} = \frac{R}{\tau_r}\left(1 - \frac{R+S+S_R}{K}\right), \tag{2.7b}$$

$$\frac{dS_R}{dt} = \frac{S_R}{\tau_r}\left(1 - \frac{R+S+S_R}{K}\right) + \frac{SR}{\tau_c} - \frac{S_R}{\tau_*}. \tag{2.7c}$$

A second model proposed in [1] extends (2.7 by assuming that P-gp is transfered through the shedding of microvessicles (MVs) by resistant cells. MVs are small particles that are released via plasma membrane blebbing. In addition to their role in mediating inflammation, coagulation, and vascular homeostasis, they are important mediators of MDR, as they facilitate cell-to-cell communication and can deliver proteins between cells [72]. The intake of MVs by sensitive cells may lead to temporary resistance. A system of ODEs that incorporates the role of MVs

(Q) in mediating MDR is written in [1] as

$$\frac{dS}{dt} = \frac{S}{\tau_s}\left(1 - \frac{R+S+S_R}{K}\right) - \frac{QS}{\tau_\eta} + \frac{S_R}{\tau_*}, \tag{2.8a}$$

$$\frac{dR}{dt} = \frac{R}{\tau_r}\left(1 - \frac{R+S+S_R}{K}\right), \tag{2.8b}$$

$$\frac{dS_R}{dt} = \frac{S_R}{\tau_r}\left(1 - \frac{R+S+S_R}{K}\right) + \frac{QS}{\tau_\eta} - \frac{S_R}{\tau_*}, \tag{2.8c}$$

$$\frac{dQ}{dt} = \lambda_1 R - \lambda_2 S\left(\frac{Q}{Q_{th}+Q}\right). \tag{2.8d}$$

In addition to introducing the mathematical models, Durán *et al.* conducted experiments on mixed cultures of NCI-H460 cell line (human non-small cell lung carcinoma) cells and NCI-H460/R resistant cells that were selected from NCI-H460 cells after three months of doxorubicin selective pressure. Cultures of only sensitive, only resistant, and mixed cultures were seeded in ratios 1:1, 3:1, and 7:1 sensitive to resistant cells and their growth was followed over time. Flow cytometry was used to measure P-gp expression levels at time points 0, 24, 48, 72, and 96 hours, and P-gp transfer was analyzed every 24 hours. The experimental data was used to calibrate the parameters of the mathematical models.

Pasquier *et al.* [49] studied cell-to-cell transfers of P-gp in co-cultures combining a sensitive human breast cancer MCF-7 cell line, and a P-gp overexpressed variant, selected for its resistance towards doxorubicin. Pasquier *et al.* derived a Boltzmann type integro-partial differential equation structured by a continuum variable corresponding to P-gp activity. The model was used to quantify the trans-

fer of P-gp activity and, in conjunction with the experimental data, to confirm the cell-to-cell transfer of functional P-gp. p is the continuous variable that measures resistance, with a density dependent growth term along with a transfer term T that encompasses all transfers that end with resistance level p.

$$\frac{\partial u(t,p)}{\partial t} = \rho(p)u(t,p) + 2\tau(T(u(t,\cdot)) - u(t,p)), \tag{2.9a}$$

$$u(0,p) = u_0(p) \in L^1_+(1,10^4). \tag{2.9b}$$

Here, the transfer operator $T(u)(p)$ is defined as

$$T(u)(p) = \frac{\int_{-\infty}^{\infty} u(p + f(\hat{p})\hat{p})u(p - (1 - f(\hat{p}))\hat{p})\, d\hat{p}}{\int_1^{10^4} u(\hat{p})\hat{p}\, d\hat{p}}. \tag{2.10}$$

A study extending this work to multiple transfer rules has been recently published in [3]. This study is the motivation for Chapter 5.

Chapter 3: A Cell-Cycle Model of P-gp Transfer

3.1 Introduction

In this chapter we study an extension of the Durán *et al.* [1] model (2.7) that we introduced in Chapter 2.3. The model is reproduced again below:

$$\frac{dS}{dt} = \frac{S}{\tau_s}\left(1 - \frac{R+S+S_R}{K}\right) - \frac{SR}{\tau_c} + \frac{S_R}{\tau_*}, \tag{3.1a}$$

$$\frac{dR}{dt} = \frac{R}{\tau_r}\left(1 - \frac{R+S+S_R}{K}\right), \tag{3.1b}$$

$$\frac{dS_R}{dt} = \frac{S_R}{\tau_r}\left(1 - \frac{R+S+S_R}{K}\right) + \frac{SR}{\tau_c} - \frac{S_R}{\tau_*}. \tag{3.1c}$$

Since the model (3.1) produces more accurate results than the alternate Durán *et al.* model (2.8), we use (3.1) as the reference model to which we compare our results.

In addition to introducing the mathematical models, Durán *et al.* conducted experiments on mixed cultures of NCI-H460 cell line (human non-small cell lung carcinoma) cells and NCI-H460/R resistant cells that were selected from NCI-H460 cells after three months of doxorubicin selective pressure. Cultures of only sensitive, only resistant, and mixed cultures were seeded in ratios 1:1, 3:1, and 7:1 sensitive to

resistant cells and their growth was followed over time. Flow cytometry was used to measure P-gp expression levels at time points 0, 24, 48, 72, and 96 hours, and P-gp transfer was analyzed every 24 hours. The experimental data was used to calibrate the parameters of the mathematical models.

In Fig. 3.1 we show the dynamics of the fractions of sensitive and resistant cells over time for different seeding ratios. Shown are the experimental results and simulations of (3.1). Clearly, while some general trends are common between the experimental data and the simulations, the fit is not optimal. For example, it takes about half the simulation time (50 hours) for the simulations to begin following the general growth trend of the data. Intriguingly, the microvessicle model, (2.8), produces a worse fit to the experimental data than model (3.1), [1].

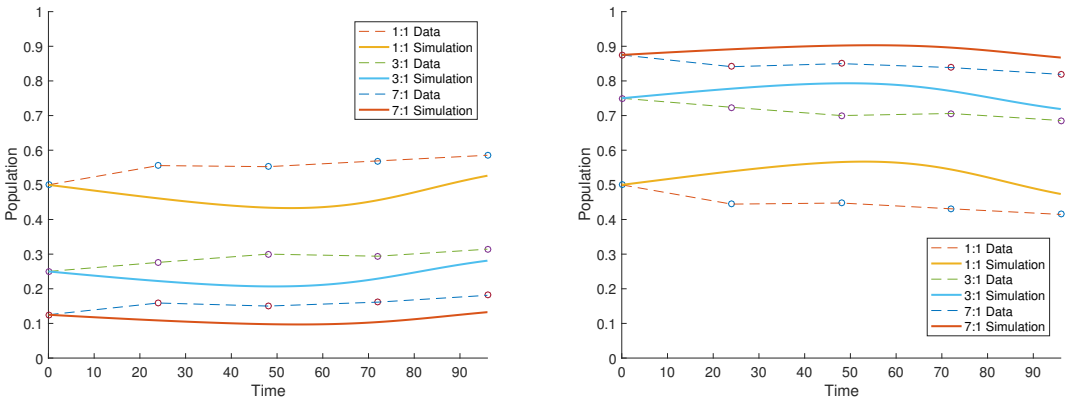

Figure 3.1: Fractions of resistant (left) and sensitive (right) cells over time. Dots correspond to the experimental data of [1]. Solid lines are simulations of the model (3.1) of [1].

Our goal in this chapter is to develop a new mathematical model for the transfer of drug resistance between cancer cell subpopulations that will provide a

better fit to the experimental data of [1]. Since neither the experiments nor models of [1] include a drug, we propose a model that incorporates no action of a drug. Building on the idea of separating the cancer cells into three subtypes: sensitive, resistant, and temporary resistant, we aim at providing a more accurate model by better capturing the cancer growth dynamics. Accordingly, we incorporate the three subpopulations into a cancer growth model of Greene *et al.* [2]. This model considers cells in three states: quiescent, proliferating, and apoptotic, with transition rates that depend on the cellular density. The model was shown in [2] to provide an accurate fit to the growth dynamics of OVCAR-8, an ovarian cancer cell line. By incorporating drug resistance and a mechanism of resistance transfer into the model of [2] we provide a better match to the NCI-H460 experimental data of [1].

The structure of this chapter is as follows: In section 3.2 we derive our new model for the P-gp transfer between cancer cells. Simulations of the model and a sensitivity study of the model parameters are shown in section 3.3. Concluding remarks are provided in section 3.4. The results presented in this chapter were published in [73].

3.2 Our Model

Our starting point is the cancer growth model of Greene *et al.* [2]. In this model, cancer cells are divided into three compartments: proliferating (P), quiescent (Q), and apoptotic (A) cells (see Fig. 3.2). The transition rates between the compartments are assumed to depend on the cellular density. Quiescent cells can

either remain quiescent, start proliferating, or commit apoptosis. Proliferating cells complete the cell cycle unless they transition to apoptosis. Once the cell cycle is completed and a cell divides, both cells transition to the quiescent compartment. Once a cell commits to apoptosis, it stays in the apoptotic compartment until it dies. The duration of the cell-cycle is assumed to be normally distributed, and the time spent in the apoptotic cycle follows a gamma distribution. The model was designed to predict variations in growth as a function of the intrinsic heterogeneity originating from the varying duration of the cell-cycle and apoptosis. The model parameters were fitted in [2] to experimental data coming from OVCAR-8, an ovarian cancer cell line. However, the model is generic and could be used to describe the growth of other cancers.

To describe resistance transfer during cancer growth, we incorporate drug resistance into the PQA model of [2]. We split the quiescent compartment, Q, into sensitive (S_q) and resistant (R_q) subtypes. The proliferative compartment, P, is also divided into sensitive (S_p) and resistant (R_p) cells. In addition, the proliferative compartment also includes a temporarily resistant phenotype (T_p). Similarly to the original PQA model, we leave the apoptotic stage as a single compartment since we assume that cells that enter apoptosis are committed to it. In our model the transfer of P-gp happens as the quiescent cells start proliferating. We assume that once cells have begun proliferating they maintain their phenotype. We define ξ to be the fraction of sensitive quiescent cells that become temporarily resistant as they transition to a proliferating state. Since P-gp transfer only leads to temporary resistance we stipulate that the progeny of temporarily resistant cells are sensitive

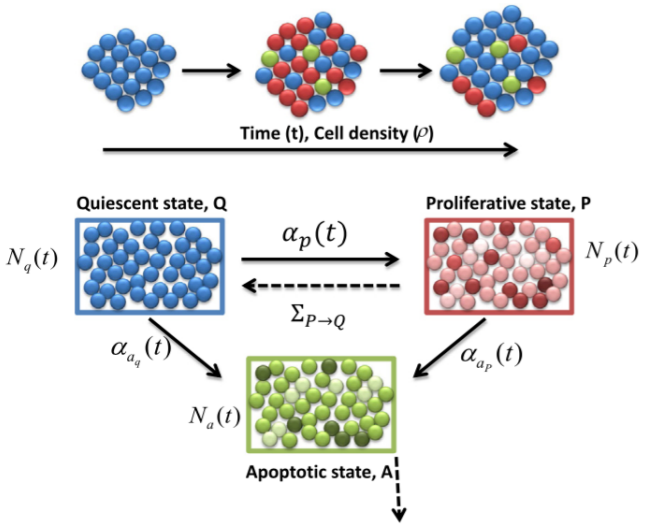

Figure 3.2: Diagram representing the PQA model from [2]. Here, P denotes the proliferative compartment, with $N_P(t)$ cells at time t. Proliferating cells can either transition to apoptosis, A, or to quiescence Q, upon completion of the cell-cycle. At time t there are $N_A(t)$ apoptotic cells and $N_Q(t)$ quiescent cells. Quiescent cells can either transition to P with rate $\alpha_p(t)$, or to A with rate $\alpha_{a_q}(t)$. The implicit transition rates due to the completion of the cell cycles are shown in dashed lines.

cells. The amount of P-gp in a temporarily resistant proliferating cell is divided between the daughter cells so we consider both offsprings to be sensitive. Clearly, a more accurate model can include a larger range of resistance levels (temporary or permanent). With the rather limited experimental data at our disposal, we prefer the simpler approach presented here. A diagram corresponding to our model is shown in Fig. 3.3.

Two equivalent model formulations were introduced in [2]: a stochastic agent-based model, and an integro-differential (IDE) model. In this chapter we choose to work with the IDE model and extend it to incorporate drug resistance. Our model equations are written as a system of six IDEs. The first two equations provide the dynamics of the quiescent cells:

$$\begin{aligned}
\frac{dS_q}{dt} &= -\alpha_{sp}S_q(t) - \alpha_{as_q}S_q(t) \\
&\quad +2\int_0^t f_p(t-t_*;\mu_1,\sigma_1)(1-\xi)\alpha_{sp}S_q(t_*)\left(1-\int_{t_*}^t \alpha_{as_p}(s)ds\right)dt_* \\
&\quad +2\int_0^t f_p(t-t_*;\mu_2,\sigma_2)\xi\alpha_{sp}S_q(t_*)\left(1-\int_{t_*}^t \alpha_{as_p}(s)ds\right)dt_*, \qquad (3.2)\\
\frac{dR_q}{dt} &= -\alpha_{rp}R_q(t) - \alpha_{ar_q}R_q(t) \\
&\quad +2\int_0^t f_p(t-t_*;\mu_2,\sigma_2)\alpha_{rp}R_q(t_*)\left(1-\int_{t_*}^t \alpha_{ar_p}(s)ds\right)dt_*.
\end{aligned}$$

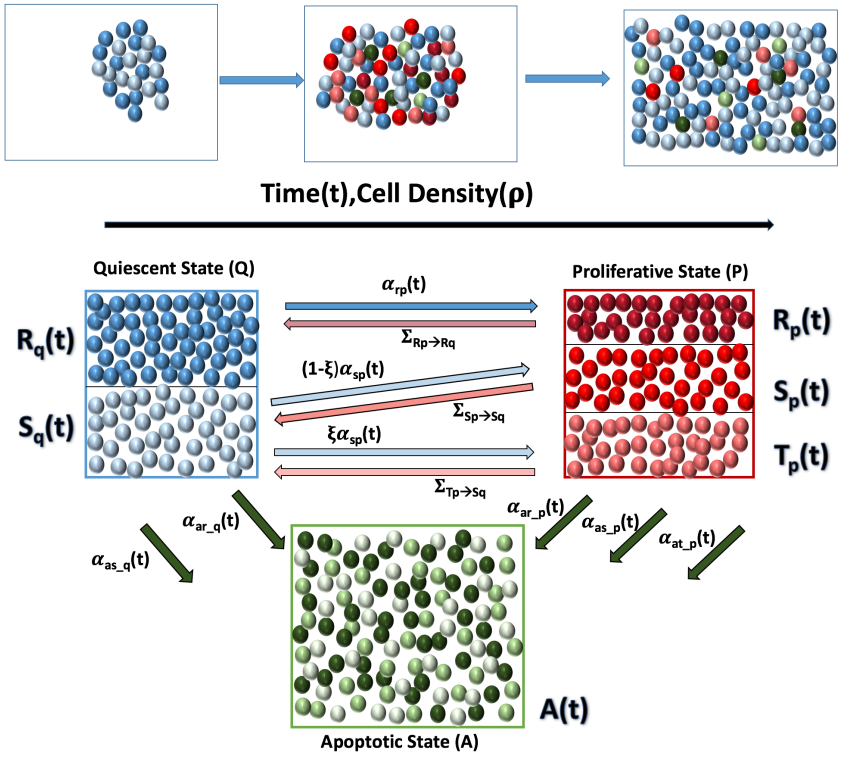

Figure 3.3: Diagram representing the proposed model (3.2)–(3.4). The quiescent cells, Q, are divided into two types: resistant quiescent cells, $R_q(t)$, sensitive quiescent cells, $S_q(t)$. The proliferating cells, P, are divided into three compartments: resistant proliferating cells, $R_p(t)$, temporary resistant proliferating cells, $T_p(t)$, and sensitive proliferating cells, $S_p(t)$. Resistant proliferating cells become resistant quiescent cells upon completing the cell cycle. Sensitive and temporary resistant proliferating cells become sensitive quiescent cells when they complete the cell cycle. Proliferating and quiescent cells may become apoptotic cells, a compartment they leave only when they die. The time spent in the proliferating cycle is normally distributed with parameters that may vary depending on whether the proliferating cells are resistant or not.

Three equations follow the dynamics of proliferating cells:

$$\begin{aligned}
\frac{dS_p}{dt} &= (1-\xi)\alpha_{sp}S_q(t) - \alpha_{as_p}S_p(t) \\
&\quad - \int_0^t f_p(t-t_*;\mu_1,\sigma_1)(1-\xi)\alpha_{sp}S_q(t_*)\left(1-\int_{t_*}^t \alpha_{as_p}(s)ds\right)dt_*, \\
\frac{dR_p}{dt} &= \alpha_{rp}R_q(t) - \alpha_{ar_p}R_p(t) \\
&\quad - \int_0^t f_p(t-t_*;\mu_2,\sigma_2)\alpha_{rp}R_q(t_*)\left(1-\int_{t_*}^t \alpha_{ar_p}(s)ds\right)dt_*, \\
\frac{dT_p}{dt} &= \xi\alpha_{sp}S_q(t) - \alpha_{at_p}T_p(t) \\
&\quad - \int_0^t f_p(t-t_*;\mu_2,\sigma_2)\xi\alpha_{sp}S_q(t_*)\left(1-\int_{t_*}^t \alpha_{at_p}(s)ds\right)dt_*.
\end{aligned} \tag{3.3}$$

A sixth equation describes the dynamics of apoptotic cells:

$$\begin{aligned}
\frac{dA}{dt} &= \alpha_{as_q}S_q(t) + \alpha_{ar_q}R_q(t) + \alpha_{as_p}S_p(t) + \alpha_{ar_p}R_p(t) + \alpha_{at_p}T_p(t) \\
&\quad - \int_0^t f_a(t-t_*)\alpha\, N(t_*)dt_*.
\end{aligned} \tag{3.4}$$

The first equation in (3.2) follows the dynamics of the sensitive quiescent cells, S_q. The first term on the RHS, $-\alpha_{sp}S_q(t)$, corresponds to the fraction of cells lost as a result of the transition to the proliferative compartment P. This term encompasses cells that stay sensitive and those that become temporarily resistant. The second term, $\alpha_{as_q}S_q(t)$, corresponds to the loss as a result of the transition to apoptosis. The integral term

$$2\int_0^t f_p(t-t_*;\mu,\sigma)\alpha_{sp}S_q(t_*)\left(1-\int_{t_*}^t \alpha_{as_p}(s)ds\right)dt_*$$

corresponds to the increase in S_q due to the progeny of the sensitive proliferating cells. We assume that all proliferating cells originated from quiescent cells, so $\alpha_{sp}S_q(t_*)$ includes all sensitive proliferating cells. There are two such terms, the first (with $1-\xi$) corresponds to sensitive proliferating cells that competed their proliferating cycle (hence the factor of 2 in front of the integral). The second term (with ξ)

corresponds to temporary resistant cells that completed their proliferation cycle and became sensitive quiescent cells. We assume that the time spent in the proliferative compartment is normally distributed with mean μ and standard deviation σ, both measured in hours,

$$f_p(t;\mu,\sigma) = \frac{1}{\sqrt{2\pi}\sigma} e^{-\frac{(t-\mu)^2}{2\sigma^2}}. \tag{3.5}$$

The term $1 - \int_{t_*}^{t} \alpha_{as_p}(s)ds$ describes the cells in the cell cycle that did not move to apoptosis before completing the proliferation cycle, where t corresponds to the time cells entered the proliferating compartment. Overall, the full integral accounts for the progeny for the proliferating cells whose time spent in the cell cycle has come to an end. The somewhat complex bookkeeping in this model (expressed by the integral terms) is due to assuming a distribution on the time cells may take to proliferate (and die), as opposed to the more standard approach of assuming that these values are constant. We allow the proliferation time, characterized by the parameters of the normal distribution, μ and σ, to differ between the resistant and sensitive populations since resistant cells may have a slower proliferation rate [74]. If these parameters are assumed to be identical for resistant and sensitive cells, both integrals terms can be combined into one term.

The second equation in (3.2) describes the dynamics of the resistant quiescent population, R_q. The RHS is similar to the first equation, with a loss term due to transition into the cell cycle and another loss term due to transition to apoptosis. Since we assume that these cells exhibit a resistant genotype we do not allow them to lose their resistance and so the integral term represents the progeny from all the

resistant cells in the cell cycle that have their time span end at a certain time t.

Similar equations are provided for the three types of cells in the proliferative compartment, described in (3.3). The first term on the RHS of the first equation for the sensitive proliferative population, S_p, represents the fraction of sensitive quiescent cells that started proliferating but stayed sensitive and did not acquire any temporary resistance. We include an apoptotic term and the same integral seen in (3.2), representing the end of the cell cycle in which each proliferating cell that has not transitioned into apoptosis divides into two new quiescent cells. The second equation, for the resistant proliferating cells, R_p, includes a transition term from resistant quiescent to resistant proliferative and another term representing transition to apoptosis term with the integral from the second equation in (3.2) showing the loss due to division at the end of the cell cycle, as cells transition to the resistant quiescent cells compartment. The third equation, for the temporary resistant proliferating cells, T_p, has the same three types of terms, with ξ multiplying the transition term from sensitive quiescent showing the fraction of cells that acquired temporary resistance.

Finally, (3.4) describes the apoptotic compartment. Once cells start apoptosis we no longer distinguish between resistant or sensitive cells. Equation (3.4) includes the five growth terms that correspond to the transitions from all compartments in (3.2)–(3.3). The length of time spent in apoptotic state is assumed to be a Gamma distribution,

$$f_a(t) = \frac{\lambda^\omega}{\Gamma(\omega)} t^{\omega-1} e^{-\lambda t}, \tag{3.6}$$

with λ and γ the rate and shape parameters of the apoptotic process and $\Gamma(\cdot)$ the gamma function. Once cells complete the time committed to apoptosis, they are removed from the system. The integral term describes this removal for all cells that die at time t. In this term we denote the total loss by $\alpha\, N(t) := \alpha_{as_q} S_q(t) + \alpha_{ar_q} R_q(t) + \alpha_{as_p} S_p(t) + \alpha_{ar_p} R_p(t) + \alpha_{at_p} T_p(t)$.

The transitions rates from [2] are functions of $\beta(\rho)$ and d, the equilibrium fraction of proliferating cells and the fraction in apoptosis, which we take to be constant. We set β_m and ρ_m as the maxima for β, and ρ, respectively, and define

$$\beta(\rho) = \begin{cases} \beta_m e^{-a(\rho-\rho_m)^2/\rho(1+\epsilon-\rho)^2} & \text{if } 0 < \rho < 1+\epsilon, \\ 0 & \text{otherwise.} \end{cases} \tag{3.7}$$

Here, ϵ is a parameter governing the shape of $\beta(\rho)$, and

$$a = \frac{\epsilon \log(\beta_m/d)}{(1-\rho_m)^2}. \tag{3.8}$$

We define the transitions $\alpha_{sp}(t)$ and $\alpha_{rp}(t)$ as the rates from sensitive quiescent to sensitive or temporarily resistant proliferating and resistant quiescent to resistant proliferating, respectively. We make the assumption that P-gp expression is independent of the transition. Hence, we set $\alpha_{sp}(t) = \alpha_{rp}(t)$. The intrinsic death terms from quiescent to apoptotic are $\alpha_{as_q}(t)$ and $\alpha_{ar_q}(t)$, with the death terms from proliferative to apoptotic being $\alpha_{as_p}(t)$,$\alpha_{ar_p}(t)$, and $\alpha_{at_p}(t)$. We again consider no effect of P-gp transfer on these terms and thus have $\alpha_{as_q}(t) = \alpha_{ar_q}(t)$ and

$\alpha_{as_p}(t) = \alpha_{ar_p}(t) = \alpha_{at_p}(t)$. These transition rates are shown below.

$$\alpha_{sp}(t) = \alpha_{rp}(t) = c\frac{(\beta(\rho(t))N(t) - P(t))_+}{Q(t)}, \tag{3.9}$$

$$\alpha_{as_p}(t) = \alpha_{ar_p}(t) = \alpha_{at_p}(t) = c\gamma\frac{(dN(t) - A(t))_+}{P(t)}, \tag{3.10}$$

$$\alpha_{as_q}(t) = \alpha_{ar_q}(t) = c(1-\gamma)\frac{(dN(t) - A(t))_+}{Q(t)}. \tag{3.11}$$

Here, $Q(t)$, $P(t)$, and $A(t)$ are the total number of cells in each respective compartment and $N(t) = Q(t) + P(t) + A(t)$ with $\rho(t) = N(t)/K$ for a carrying capacity K. The transition from Q to P is a function of the difference between the current proliferative population, $P(t)$, and the desired (or equilibrium) proliferative population, $\beta(\rho(t))N(t)$. Similarly, the transitions into apoptosis are functions of the difference between current apoptotic population $A(t)$, and desired fraction in apoptosis $dN(t)$, where d is taken to be a small constant < 0.05. c is the cellular reaction rate and γ describes the rate difference between the proliferating cells and quiescent cells when going into apoptosis.

3.3 Results

3.3.1 Numerical Methods

We use a four-step explicit Adams-Bashforth (AB) method to approximate solutions of the system (3.2)–(3.4). This solver is chosen since it does not require temporary intermediate values, which simplifies the calculations due to the presence of the integral terms. The method can be written as

$$y_{n+1} = y_n + \frac{\Delta t}{24}(55f_n - 59f_{n-1} + 37f_{n-2} - 9f_{n-3}), \tag{3.12}$$

with lower degree AB methods for the first 3 steps. Integrals of the form

$$\int_0^t h_1(t,t_*)\left(1-\int_{t_*}^t h_2(s)ds\right)dt_* \tag{3.13}$$

are discretized using the same time steps used with the AB method (3.12). If we denote

$$I(t,t_*)=\int_{t_*}^t h_2(s)ds,$$

we can approximate $I(t+\Delta t,t_*)$ with

$$\begin{aligned} I(t+\Delta t,t_*)&=\int_{t_*}^{t+\Delta t} h_2(s)ds=\int_{t_*}^{t} h_2(s)ds+\int_{t}^{t+\Delta t} h_2(s)ds\\ &\approx \int_{t_*}^{t} h_2(s)ds+h_2(t)\Delta t=I(t,t_*)+h_2(t)\Delta t. \end{aligned} \tag{3.14}$$

Equation (3.14) requires only one function evaluation. The complete integral (3.13) is then evaluated with a composite trapezoidal rule on a uniform grid:

$$\begin{aligned} \int_0^t h_1(t,t_*)\left(1-\int_{t_*}^t h_2(s)ds\right)dt_* \approx \frac{\Delta t}{2}\sum_{k=1}^{N}&\left(h_1(t,t_k)(1-I(t,t_k))\right.\\ &\left.+\,h_1(t,t_{k+1})(1-I(t,t_{k+1}))\right), \end{aligned} \tag{3.15}$$

with t_k the kth point and N the size of the discretization.

In our simulations, we optimized the model parameters using Matlab's nonlinear least squares function, fitting the solution of (3.2)–(3.4) to the experimental data of [1]. We set $d=0.03$, which corresponds to the same fraction of cells in apoptosis from [2]. The full list of parameters and their ranges is given in Table 3.1. The optimal values used in the simulations are given in Table 3.2 for the case in which resistant cells and sensitive cells have different growth parameters, and in Table 3.3 for the case when the growth parameters are identical for both sensitive and resistant cells.

Table 3.1: Parameter Values & Descriptions

Parameter	Range	Description	Reference
t	[0,180] (hours)	Time	[1]
μ_1	[10,∞) (hours)	Mean length of (sensitive) cell cycle	[2]
σ_1	[0,10] (hours)	Standard deviation of (sensitive) cell cycle	[2]
μ_2	[12,∞) (hours)	Mean length of (resistant) cell cycle	[2]
σ_2	[0,10] (hours)	Standard deviation of (sensitive) cell cycle	[2]
ω	4.9436	Shape parameter of entire apoptotic process	[2]
λ	0.19117 (per hour)	Rate parameter of entire apoptotic process	[2]
$\rho(t)$	$[0, \infty)$	Density of cells at time t	[2]
K	7.5×10^5	Carrying capacity	[1]
d	[0.01,0.05]	Fraction of cells in apoptosis	[2]
$\beta(\rho)$	[0,1]	Fraction in cell cycle as a function of density	[2]
β_m	[0,1]	Maximum of $\beta(\rho)$	[2]
ρ_m	[0,1]	Maximizing density of $\beta(\rho)$	[2]
ϵ	$[0, \infty)$	Parameter governing shape of $\beta(\rho)$	[2]
c	$[0, \infty)$ (per hour)	Cellular reaction rate	[2]
γ	[0,1]	Rate difference between α_{ap} and α_{aq}	[2]
ξ	[0,1]	Fraction of cells becoming temporarily resistant	

Table 3.2: Parameters values used in simulations with different growth parameters for the sensitive and resistant cells

Parameter	μ_1	σ_1	μ_2	σ_2	ω	λ	K
Value	10.0258	9.2818	12.0033	5.8467	4.9436	0.19117	7×10^5
Parameter	d	β_m	ρ_m	ϵ	c	γ	ξ
Value	0.03	0.8	0.0458	0	15.4753	0.8331	0.0412

Table 3.3: Parameters Values Used in Simulations with identical growth parameters for the sensitive and resistant cells

Parameter	μ_1	σ_1	μ_2	σ_2	ω	λ	K
Value	10.2365	4.3263	10.2365	4.3263	4.9436	0.19117	7×10^5
Parameter	d	β_m	ρ_m	ϵ	c	γ	ξ
Value	0.03	0.8	0.2	0.2346	1.6732	0.5011	0.4828

3.3.2 Simulations

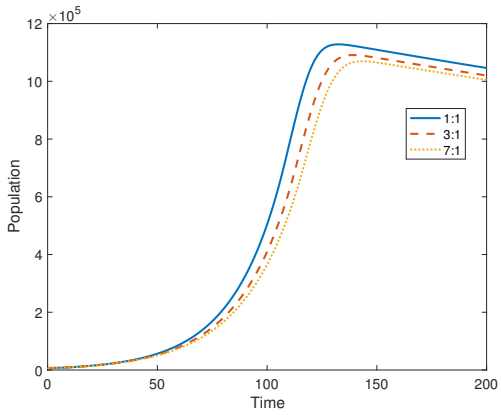

Figure 3.4: The dynamics of the total population of resistant and sensitive cells over 200 hours simulated with (3.2)–(3.4). We consider the three initial ratios of sensitive to resistant cells: 1:1, 3:1, and 7:1.

Our first simulations show the total population of sensitive and resistant cells over time for three different initial conditions. Following the setup of [1] we run separate simulations for a 1:1, 3:1, and 7:1 initial ratio of sensitive to resistant cells. The resistant subtype, as described in [1], are cells that have been given Doxorubicin for three months and survived. At time $t = 0$ all cells are assumed to be quiescent. Fig. 3.4 shows growth up to a carrying capacity and then a small decline, which compares well to the data shown in [1]. The trend of the population growth is similar in all three cases.

We next look at the how the fractions of sensitive and resistant cells change over time. The results are shown in Fig. 3.5. We compared simulations of our model (3.2)–(3.4) with simulations of the model of [1] given by (3.1). The simulations

results are plotted on top of the experimental data of [1]. A comparison between the results produced by both models shows that the new model (3.2)–(3.4) provides a substantially better match to the experimental data over the simulated 96 hours, compared with the model (3.1), both in terms of the absolute error, as well as the overall trend. We see an early inflection point in our model due to the faster proliferation rate of the sensitive cells. Initially the growth of the sensitive cell fraction outpaces the resistant cell fraction. After around 12 hours the resistant cells begin to catch up. Then the transfer of resistance contributes to a rise in the fraction of resistant cells. We significantly oversampled the data to check for overfitting and the results were similar, which makes sense given the lack of observed oscillations in the experiemental data.

We test the sensitivity of the model (3.2)–(3.4) to changes in four of the parameters, d, c, ϵ, and ξ. Fig. 3.6 shows how the overall population varies when d, c, and ϵ, respectively, are changed. We ran simulations to compare how the sensitive and resistant fractions change but these result with only negligible changes so we focus on total cell population. Changes to d, the parameter governing the fraction of cells in apoptosis, are shown in the top left graph in Fig. 3.6. There is a small effect on the overall population once it has reached carrying capacity with a larger death parameter correlating with a faster decline but the system overall does not change much as d changes. The cellular reaction rate c amplifies the magnitude of cells moving from quiescent stage into the cell cycle. The simulation shown in the top right graph in Fig. 3.6 confirms that a low c value correlates with slower growth. However, for larger values of c, the growth is mostly independent of c. The

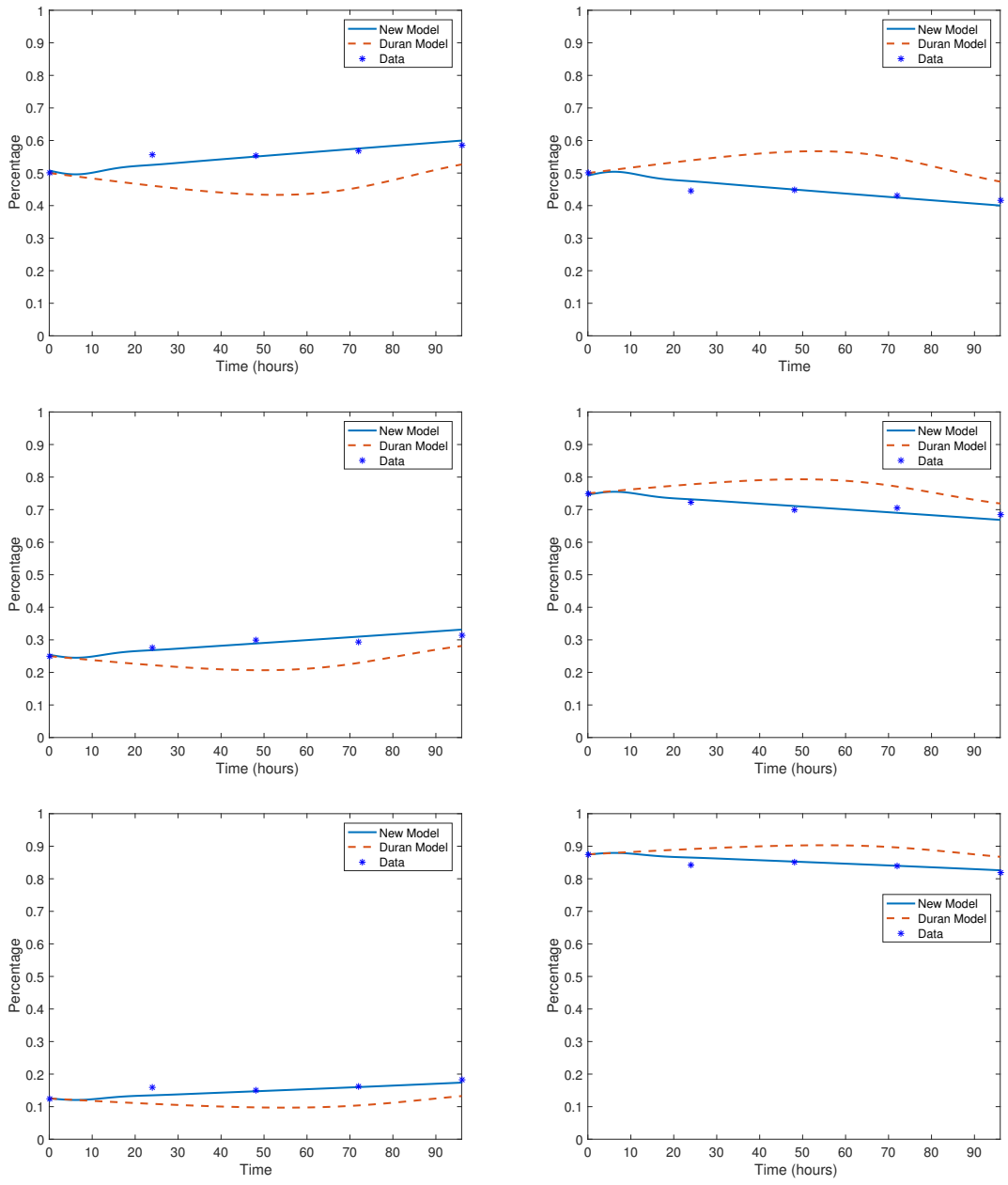

Figure 3.5: Fractions of resistant (left) and sensitive (right) cells over time. Top: initial ratio 1:1. Middle: initial ratio 3:1. Bottom: initial ratio 7:1. Dots correspond to the experimental data of [1]. Dashed lines are simulations with the model (3.1) of [1]. Solid lines are simulations of (3.2)–(3.4).

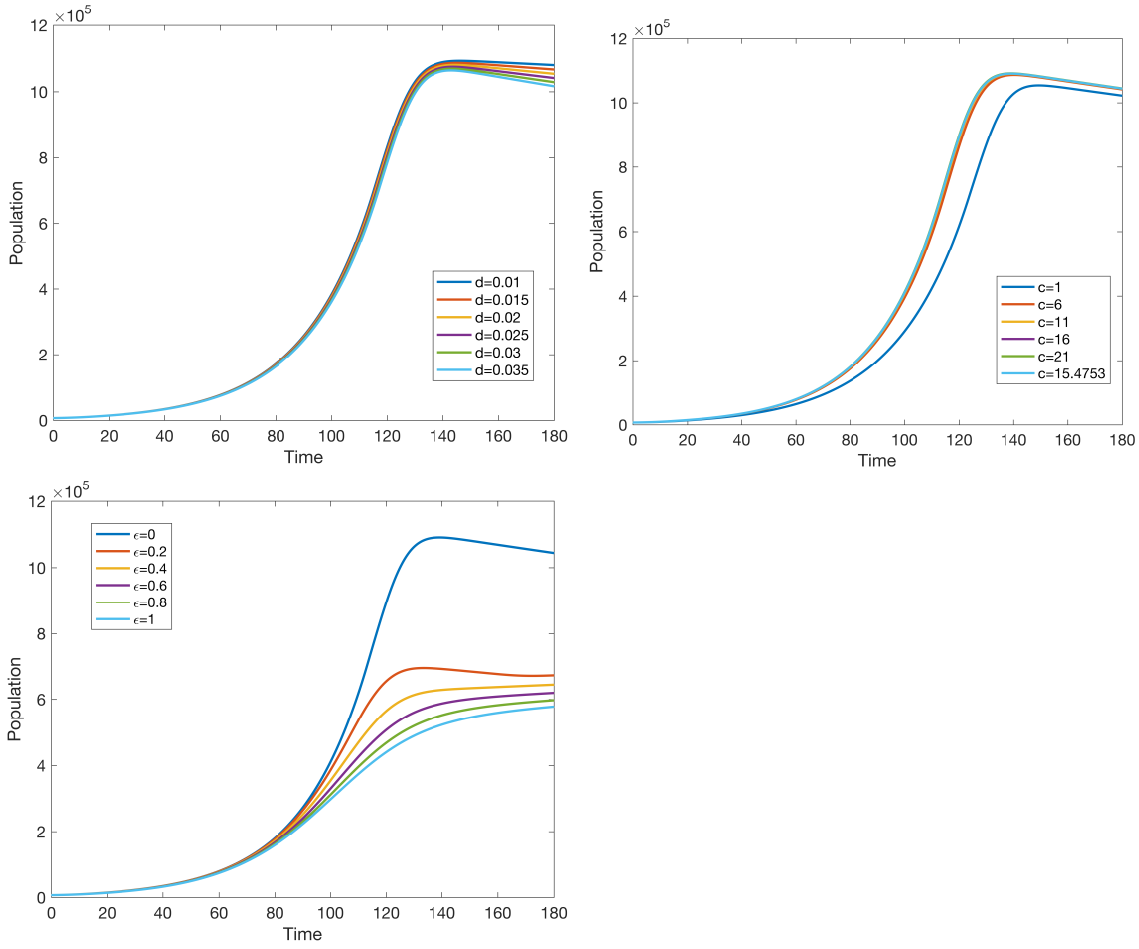

Figure 3.6: Sensitivity study of (3.2)–(3.4) for the case of an initial sensitive to resistant ratio of 3:1. All graphs show the total cell population over time. Top Left: varying d, the fraction of cells in apoptosis. Top Right: varying c, the cellular reaction rate that governs the transition from quiescent to proliferative. Bottom: varying ϵ, the shape parameter for $\beta(\rho)$.

parameter ϵ governs the shape of $\beta(\rho)$, the equilibrium, or desired, amount of cells in the cell-cycle. The bottom left graph in Fig. 3.6 demonstrates that the total population is sensitive to changes in ϵ. While the sensitive and resistant fractions remain consistent, any deviation from $\epsilon = 0$ leads to a significant decrease in the overall growth. $\epsilon = 0$ implies that $\beta(\rho) = \beta_m$, a constant. This corresponds to a lack of dependence on density. We expect this to be the best fit as the model and experimental data address a local phenomenon.

The parameter ξ, which governs the fraction of sensitive quiescent cells that become temporarily resistant as they enter the cell cycle, is the final parameter we varied. Resistant cells proliferate at a slower rate but we see that the difference is not enough to induce change on the overall population. However, there is a shift in the sensitive and resistant fractions, as would be expected. Fig. 3.7 shows the population and the two fractions while Fig. 3.8 shows a zoomed on version of Fig. 3.7 to highlight the shift towards more resistance as ξ is raised. The larger ξ is, the more cells become temporarily resistant and so the overall resistant fraction rises.

We also ran simulations in which we allowed the sensitive and resistant cells to have the same growth parameters (i.e., a normal distribution with identical mean and standard deviations for the cell cycle length). Without the slower proliferation our optimized parameters have a much larger value for ξ, the fraction of sensitive quiescent cells that become temporarily resistant. In these simulations we have almost half of them becoming resistant ($\xi = 0.4828$). The results of these simulations are shown in Fig. 3.9 (compare with Fig. 3.5 where resistant cells are assumed to grow slower than the sensitive cells). Even in this case, our model (3.2)–(3.4) provides a

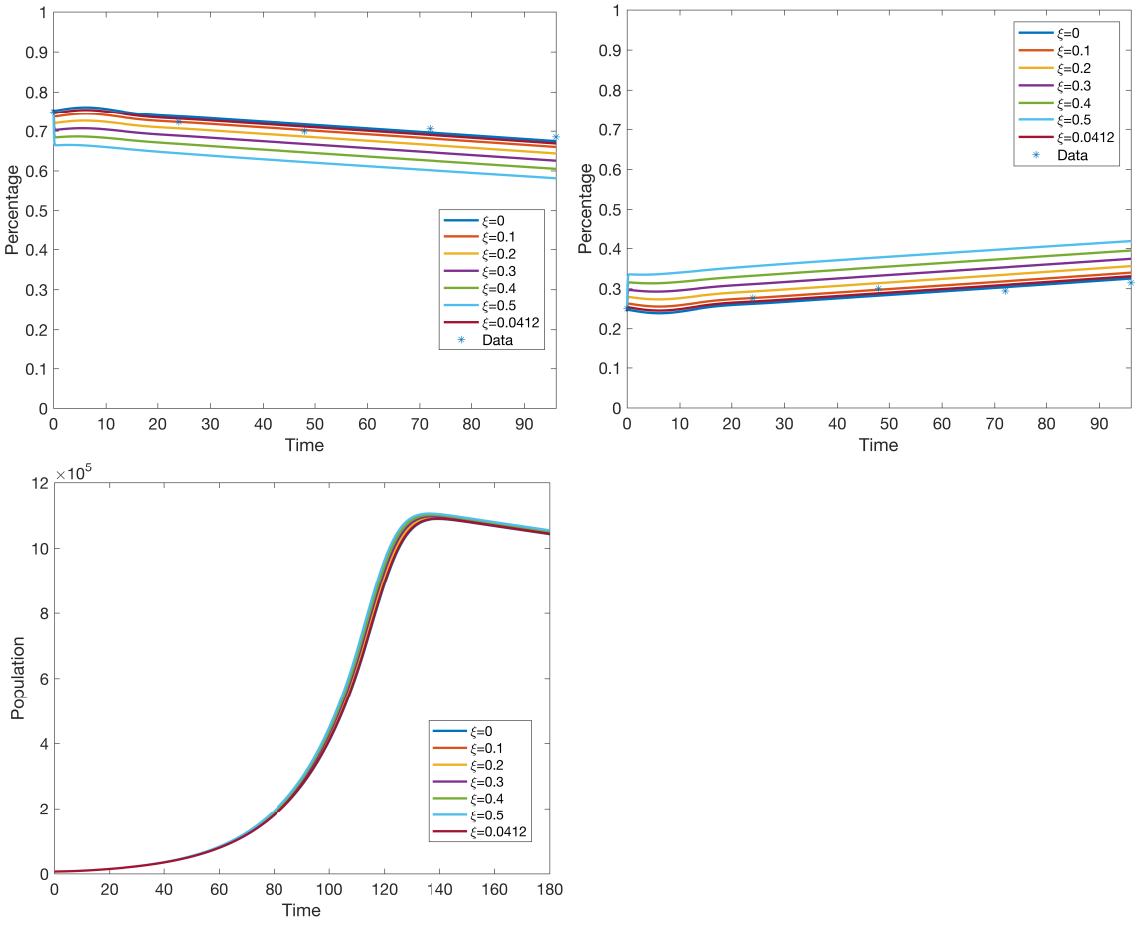

Figure 3.7: Top Left: Fraction of sensitive cells as ξ, the fraction of sensitive quiescent cells that transition to temporarily resistant when in the proliferative state, varies. Top Right: Fraction of resistant cells as ξ varies. Bottom: Total Population as ξ varies.

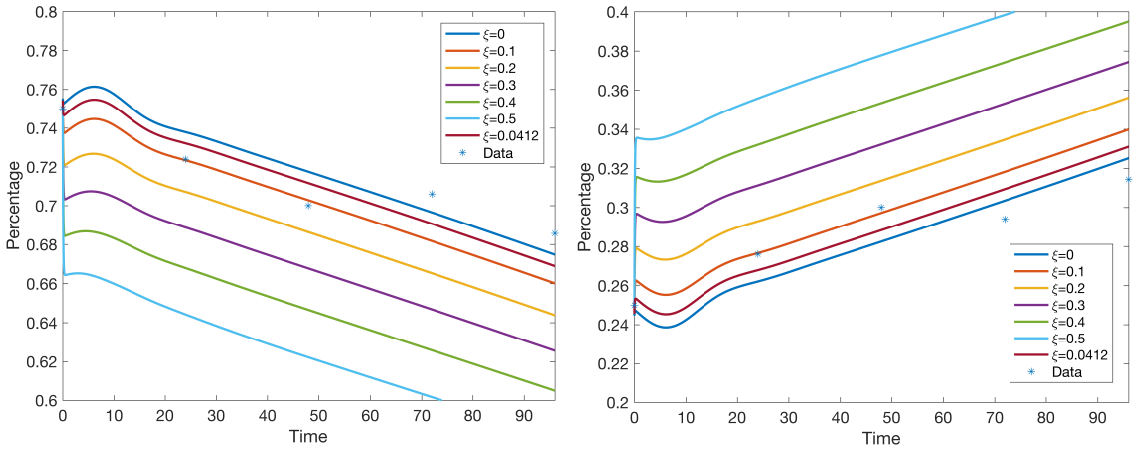

Figure 3.8: Left: A close up for the fraction of sensitive cells as ξ, the fraction of sensitive quiescent cells that transition to temporarily resistant when in the proliferative state, varies. Right: A close up for the fraction of resistant cells as ξ varies.

better match in capturing the trend of the data compared with the model of [1].

We note that the parameters are optimized based on the available experimental data that was collected over the first 96 hours. When simulating our model beyond 96 hours with identical growth distributions for the sensitive and the resistance cells, the fractions of sensitive and resistant cells trend back towards their initial values. The model (3.1) exhibits a limit dynamics in which the sensitive and resistant cells settle towards equilibrium values albeit values that are different than the initial distribution.

It is easy to understand the reason for this asymptotic behavior when the growth distributions of sensitive and resistant cells are identical. In this case, we can assume that R_p changes at a similar rate to $S_p + T_p$. When the carrying capacity

is approached, $\beta(\rho)$ gets increasingly small. This means that the transition rates from quiescence to the proliferative compartment shrink. Once all the temporarily resistant proliferating cells divide into sensitive quiescent cells, the transition rates are too small to repopulate T_p. The overwhelming majority of cells are quiescent, either resistant or sensitive. When temporary resistant cells make up a small fraction of the population, the asymptotic distribution of cells reverts to the initial values. This can all be avoided by allowing the resistant population to proliferate at a slower rate than the sensitive cells, which is a biologically solid assumption [74].

3.4 Discussion

Mathematical models of the mechanisms of cellular growth may assist in studying and understanding the emergence and evolution of MDR. The cell-to-cell transfer of P-gp and its effect have not been extensively studied by the mathematical community.

In this chapter we propose a model for the resistance transfer between cells. Our model assumes that cells are either quiescent, proliferative, or in the apoptotic stage. Cells in the quiescent and proliferative stages are designated either resistant or sensitive, with an extra compartment for temporarily resistant proliferative cells. We assume that a certain fraction of sensitive cells become temporarily resistant due to P-gp transfer as they become proliferative and enter the cell cycle. This model is an extension of the cancer growth model of Greene *et al.* [2] to which we incorporated drug resistance.

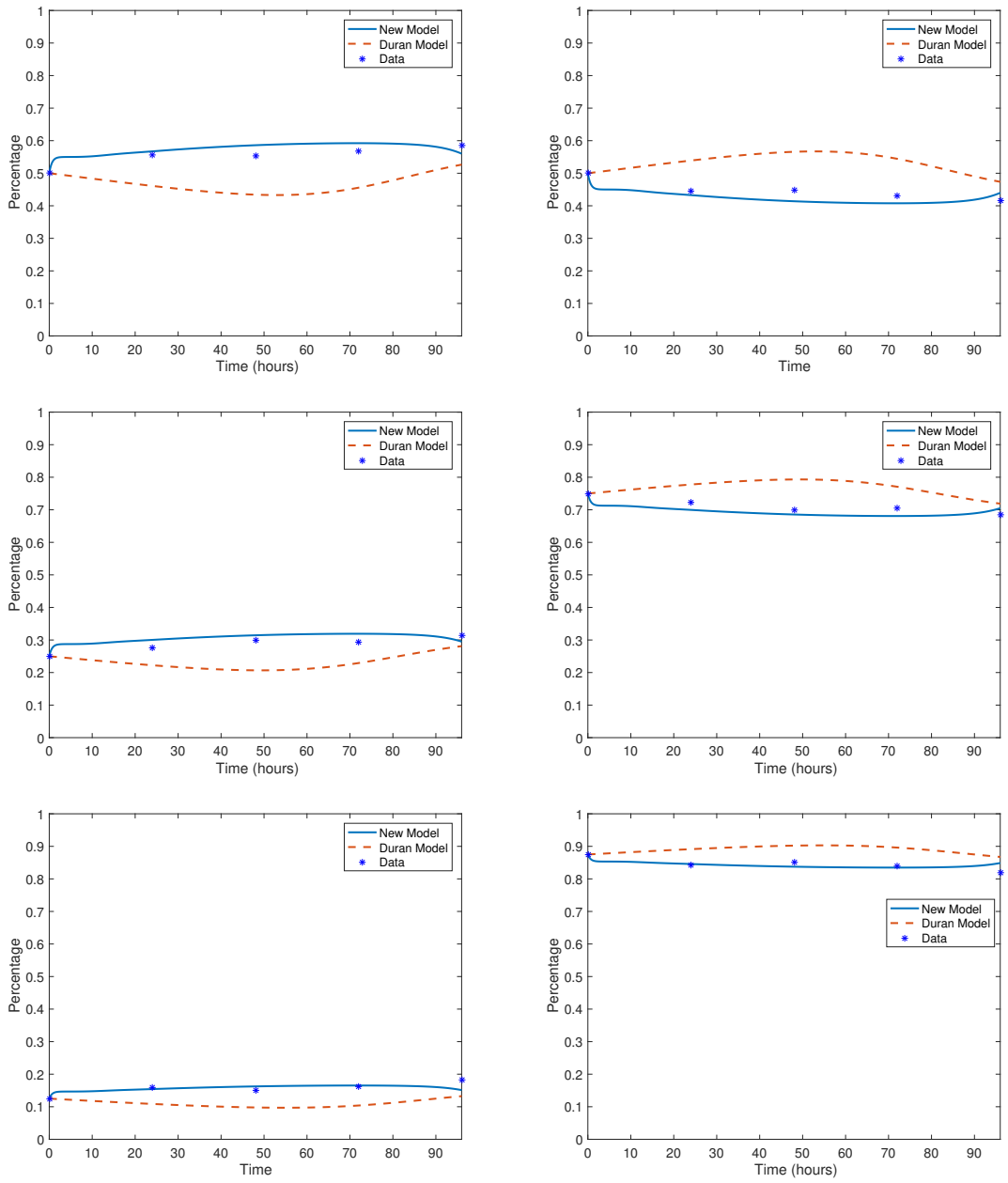

Figure 3.9: Fractions of resistant (left) and sensitive (right) cells over time assuming identical growth parameters for the sensitive and the resistant cells. The parameters used in this figure are given in Table 3.3. Top: initial ratio 1:1. Middle: initial ratio 3:1. Bottom: initial ratio 7:1. Dots correspond to the experimental data of [1]. Dashed lines are simulations with the model (3.1) of [1]. Solid lines are simulations of (3.2)–(3.4).

We fit our model to the experimental data from [1] and show that the more detailed description of the growth dynamics in our model provides a better fit to the experimental data than the fit that can be obtained using the original model of [1]. We demonstrate that a better match to the experimental data is obtained when resistant cells are allowed to grow at a different rate than the sensitive cells. The best fit is obtained when the resistant cells grow more slowly than the sensitive cells, which is consistent with known experimental data.

With this better fit our model could now potentially be used for studying a similar setup under drug treatment. Given data on sensitive and resistant responses to the action of a drug, this would be a reasonable next step.

Chapter 4: A Reaction-Diffusion Model for the Spread of Transferred Resistance

In this chapter we present another extension of Durán et. al [1]. Here we incorporate a spatial component rather than a cell-cycle model. The structure of the chapter is as follows: we begin with a simple reaction-diffusion model for resistant and sensitive cancer cells. We then add a temporarily resistant type, mirroring the model of chapter 3. We then look at a system with no P-glycoprotein transfer but the inclusion of a chemotherapeutic drug. Finally we put it all together with a model that incorporates transferred resistance alongside the mass action of the drug.

4.1 A First Model

Reaction-diffusion equations are a common type of parabolic partial differential equations. They can be applied to chemistry, biology, physics, and other dynamic processes [75]. These equations have been used in the study of pattern formation since Alan Turing's seminal work on morphogenesis [76]. The change in the concentration variable is modeled as a function of two forces, a (chemical or otherwise) reaction along with diffusion across space. We begin with a coupled reaction-diffusion system: a scaled Lotka-Volterra competition model with the ad-

dition of diffusion [77]. This system with diffusion and competition is commonly called a Fisher-KPP system (Kolmogorov, Petrovsky, and Piskunov) [78, 79].

$$\frac{\partial u}{\partial t} = D_u \Delta u + u(1 - u - v), \tag{4.1a}$$

$$\frac{\partial v}{\partial t} = D_v \Delta v + av(1 - u - v). \tag{4.1b}$$

We consider space in two dimensions x and y, thus $\Delta = \frac{\partial^2}{\partial x^2} + \frac{\partial^2}{\partial y^2}$. In this model $u(x, y, t)$ represents the density of the cancer cells sensitive to a drug, with values between 0 and 1, while $v(x, y, t)$ represents the density of the cancer cells exhibiting MDR. Each diffuses at a certain rate, D_u and D_v, respectively. Both sets of cells exhibit logistic growth limited by competition for space. We let $a < 1$ assuming that resistant cells grow slower than sensitive cells. We will revisit this assumption later in this chapter.

4.1.1 Numerical Methods

In order to simulate (4.1) we discretize the system using the finite difference method. We use n for each time step and i and j for the two spatial dimensions. The time derivatives are discretized via the forward, or explicit, Euler method, with $k = \Delta t$:

$$\frac{\partial u}{\partial t}|_{t=n} \approx \frac{u_{i,j}^{n+1} - u_{i,j}^{n}}{k}. \tag{4.2}$$

We use an implicit 5-point stencil for the finite difference approximations. In this case the (i, j) component of the Laplacian at time step n is written as

$$\Delta u \approx \frac{u_{i+1,j}^{n+1} + u_{i-1,j}^{n+1} + u_{i,j+1}^{n+1} + u_{i,j-1}^{n+1} - 4u_{i,j}^{n+1}}{h^2}, \tag{4.3}$$

where $h = \Delta x$. We take the sum of the four closest values at the next time step, $n+1$, and subtract four times the value of the (i, j) component at $t = n+1$. This is an implicit method so combined with the explicit Euler, we are using a semi-implicit method of updating each component. This allows us to solve a linear system for each $u_{i,j}^{n+1}$ and $v_{i,j}^{n+1}$. For each $u_{i,j}^{n+1}$, we have:

$$\frac{u_{i,j}^{n+1} - u_{i,j}^{n}}{k} \approx D_u \frac{u_{i+1,j}^{n+1} + u_{i-1,j}^{n+1} + u_{i,j+1}^{n+1} + u_{i,j-1}^{n+1} - 4u_{i,j}^{n+1}}{h^2} + u_{i,j}^{n}(1 - u_{i,j}^{n} - v_{i,j}^{n}). \tag{4.4}$$

We set up the discretized equation for $v_{i,j}^{n+1}$ in the same manner. In implementing the code on Matlab we utilize sparse matrices to increase the efficiency of the simulation. The simulations of the extensions of this model used in the upcoming sections all use a similar discretization.

Since we are going to use this as an extension of Durán et. al [1] in the next sections, we run a simulation assuming a 1:1 ratio of sensitive to resistant cells equally spaced in the center of a two-dimensional domain with Dirichlet boundary conditions (Figure 4.1). We set $u = 0$ and $v = 0$ on the boundary. Without the presence of a drug, the competitive advantage of the sensitive cells allows them

to quickly overtake the resistant population. What looks like a dip in sensitive population in the center is due to the population growing faster at the edge and the center eventually catching up. The plots show the respective densities after 10, 50, and 100 hours. The parameters used throughout the simulations are described in Section 4.2.1.

When we extend the simulations to two months, we see that the sensitive cells represent over 90% of the tumor in Figure 4.2, as expected. In this simple case, the only distinction between the two populations is the slower growth rate of the resistant cells, making it clear that the advantage lies with the sensitive cells.

Simulations for populations with 3:1 and 7:1 initial ratios exhibit similar, if exaggerated, characteristics. Without any external forces on this system, the resistant cells cannot overcome the sensitive cells and, while the tumor will grow to capacity, the sensitive cells will dominate.

4.1.2 Fisher's Equation

When we make two simplifying assumptions, namely that $D_u = D_v = D$, and $a = 1$, then we can rewrite the system (4.1) as follows:

$$\frac{\partial u}{\partial t} = D\Delta u + u(1 - u - v), \tag{4.5a}$$

$$\frac{\partial v}{\partial t} = D\Delta v + v(1 - u - v). \tag{4.5b}$$

Adding both equations and setting $\mu = u + v$ we get

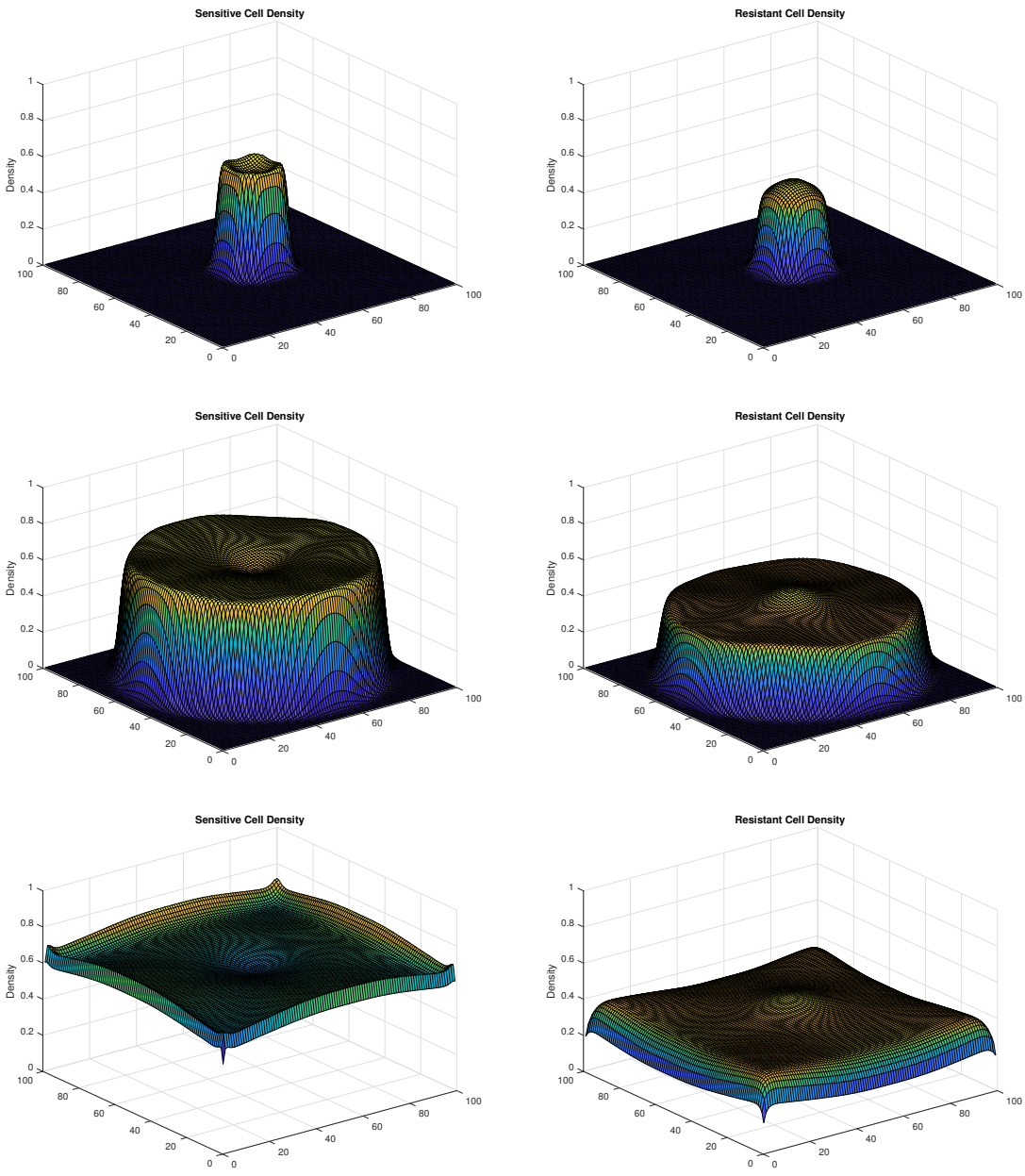

Figure 4.1: Simulation of (4.1). Densities of sensitive (left) and resistant (right) cells over time. Initial 1:1 ratio. Top: t=10 hours. Middle: t=50 hours. Bottom: t=100 hours.

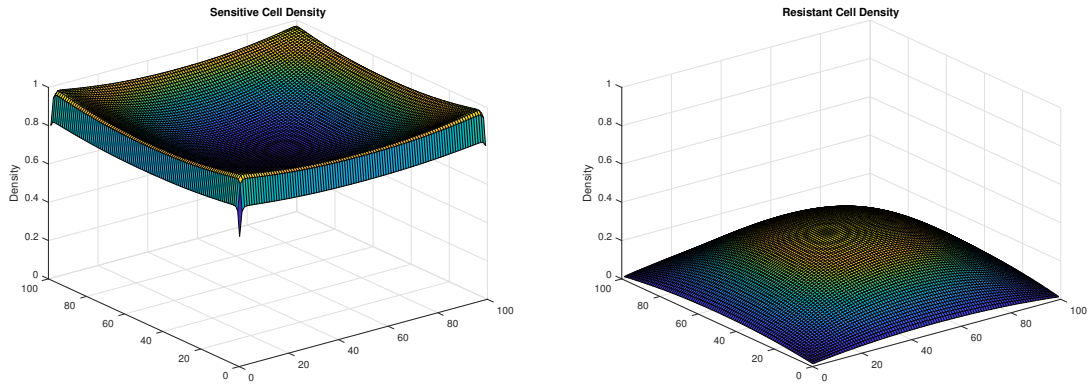

Figure 4.2: Simulation of (4.1). Densities of sensitive (left) and resistant (right) cells after two months. Initial 1:1 ratio.

$$\frac{\partial \mu}{\partial t} = D\Delta\mu + \mu(1-\mu). \tag{4.6}$$

Equation (4.6) is the classic Fisher equation, from the 1937 paper on the spread of a certain allele [78]. There are two equilibrium states, $\mu = 0$, and $\mu = 1$, and in between traveling wave solutions can exist. We can see these in Figure 4.3 as the tumor grows to the equilibrium state $\mu = 1$.

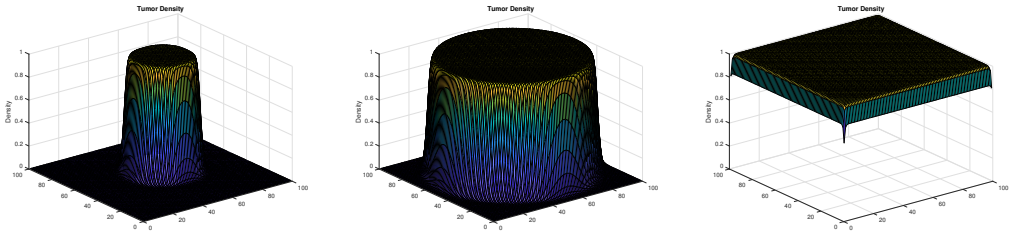

Figure 4.3: Simulation of the Fisher equation (4.6). Overall tumor density is shown over a period of 100 hours. Left: t=10 hours. Middle: t=50 hours. Right: t=100 hours.

4.2 Transferred Resistance

As discussed in Chapters 2 & 3, the overabundance of P-glycoprotein pumps leads to MDR. We understand that resistant cells can transfer P-gp pumps to nearby sensitive cells. We apply the transfer of resistance terms of [1] to (4.1) to incorporate a third equation for those temporarily resistant cells.

$$\frac{\partial u}{\partial t} = D_u \Delta u + u(1-u-v-w) - k_u uv + k_w w, \tag{4.7a}$$

$$\frac{\partial v}{\partial t} = D_v \Delta v + a_v v(1-u-v-w), \tag{4.7b}$$

$$\frac{\partial w}{\partial t} = D_w \Delta w + a_w w(1-u-v-w) + k_u uv - k_w w. \tag{4.7c}$$

Here, $w(x, y, t)$ represents temporarily resistant cells. The resistant cells transfer a small amount of P-gp pumps to nearby sensitive cells, allowing for a short-term change in the resistant phenotype. After a specified amount of time, controlled by k_w, the temporarily resistant cell turns back into a sensitive cell.

4.2.1 Simulations of The Transferred Resistance Model (4.7)

As in Chapter 3, we optimized parameters using Matlab's nonlinear least squares function. We fit the solution of (4.7) to the experimental data of [1]. To deal with the inherent scarcity of data points and concerns about overfitting we synthesized extra points using linear interpolation to confirm our results. Since we do not assume any phenotypic difference between resistant and temporarily resistant cells,

we force $a_v = a_w$ in all simulations. The full set of parameters with their ranges is given in Table 4.1. The optimal values used in the simulations are given in Table 4.2.

The results for the parameter optimization are shown in Figures 4.4 and 4.5. The top plot in Figure 4.4 shows the percentage of sensitive cells in (4.7) over 100 hours against the experimental data. For comparison, the bottom plot shows the simulations of (3.2)-(3.4) and of [1] against the same experimental data. Whereas (3.2)-(3.4), while originally a great improvement, had a small jump in percentage followed by a linear decline, (4.7) follows the data much more closely. We can see similar effects in Figure 4.5 for resistant cells, which in all cases include both permanently and temporarily resistant cells. Using these parameters we now can look at further growth dynamics.

We see the growth of the system over those same 100 hours in Figure 4.6. We start with an equal amount of sensitive and resistant cells spaced in a small grid in the center of our domain. We set no initial temporarily resistant cells and keep $u = 0, v = 0, w = 0$ as the Dirichlet boundary condition. In the top row of Figure (4.6) we see an initial depletion of sensitive cells due to the transfer of P-gp from the nearby resistant cells. Meanwhile on the edge of the initial population the sensitive cells grow faster than the resistant cells due to their competitive advantage. After 100 hours we see that the relative sizes of each population are almost uniformly dispersed throughout our domain. The optimized transfer terms were $k_u = 0.1150$ and $k_w = 0.0757$, agreeing with common understanding that the transfer of P-gp is not an overwhelming aspect of the system. Despite the existence of temporarily

Table 4.1: Parameter Values & Descriptions

Parameter	Range	Description
t_{end}	[0,1460] (hours)	Length of Time Interval
N_z	[10, 1000]	Length of one side of square domain
dt	[0.1,10] (hours)	Length of discretized time step
dz	[0.1,10]	Length of spatial step
D_u	[0.05,5]	Diffusion coefficient for sensitive cells
D_v	[0.05,5]	Diffusion coefficient for resistant cells
D_w	[0.05,5]	Diffusion coefficient for temporarily resistant cells
D_c	[0.05,∞)	Diffusion coefficient for the drug
ϵ	[0,∞)	Scaling parameter for drug diffusion
a_v	$[0.5, 0.85]$	Growth parameter for resistant cells
a_w	$[0.5, 0.85]$	Growth parameter for temporarily resistant cells
d_u	$[0.8, 1]$	Death parameter of sensitive cells due to drug
d_v	$[0.1, 0.5]$	Death parameter of resistant cells due to drug
d_w	$[0.1, 0.5]$	Death parameter of temporarily resistant cells due to drug
γ	[0,1]	Inherent decay rate of drug
λ_u	[0,1]	Drug uptake parameter for sensitive cells
λ_v	[0,1]	Drug uptake parameter for resistant cells
λ_w	[0,1]	Drug uptake parameter for temporarily resistant cells
k_u	$[0.01, 0.2]$	P-gp transfer parameter for sensitive and resistant cell interaction
k_w	$[0.01, 0.2]$	Reversion parameter for temporarily resistant back to sensitive

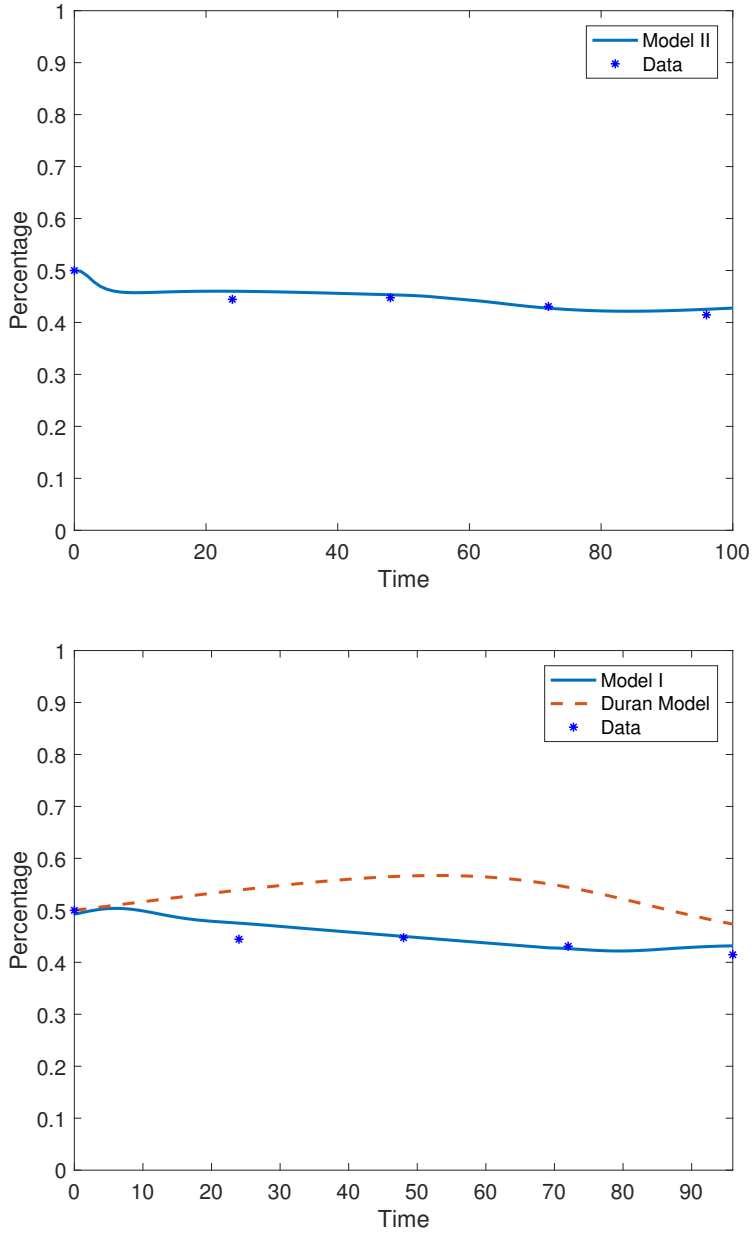

Figure 4.4: Fractions of sensitive cells over time assuming a 1:1 initial ratio. Dots correspond to the experimental data of [1]. Top: simulation of the model (4.1). Bottom: a dashed line simulation of the model (3.1) of [1] and a solid line simulation of (3.2)-(3.4).

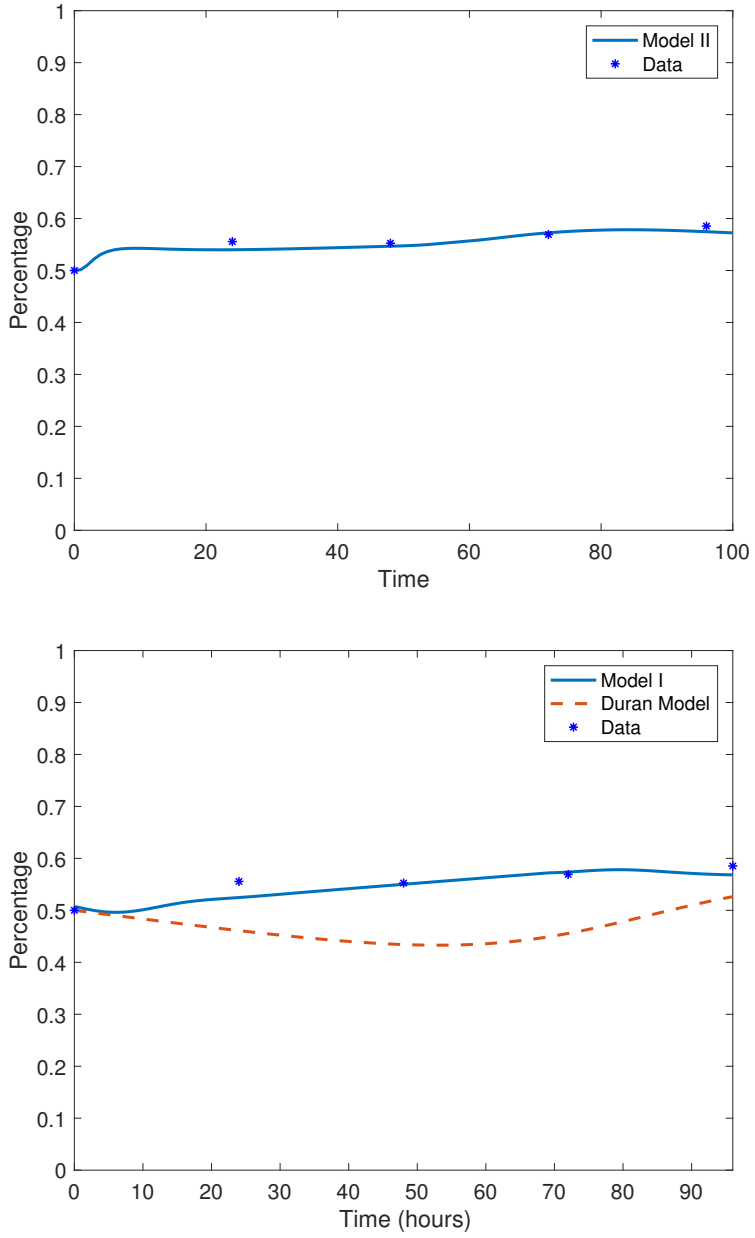

Figure 4.5: Fractions of resistant cells over time assuming a 1:1 initial ratio. Dots correspond to the experimental data of [1]. Top: simulation of the model (4.1). Bottom: a dashed line simulation of the model (3.1) of [1] and a solid line simulation of (3.2)-(3.4).

Table 4.2: Parameters values used in simulations with $D_v \neq D_w$.

Parameter	N_z	dt	dz	D_u	D_v	D_w	D_c
Value	101	1	0.5	0.05	0.0592	0.0585	1
Parameter	ϵ	a_v	a_w	d_u	d_v	d_w	γ
Value	0.5	0.85	0.85	0.85	0.2	0.2	0.4
Parameter	λ_u	λ_v	λ_w	k_u	k_w		
Value	0.5	0.05	0.05	0.1150	0.0757		

resistant cells, the dominant growth term of the sensitive cells still allows them to win over the resistant cells. This is further seen in Figure 4.7, which shows the system after two months. As with the case with no temporary resistance, the supermajority of cells are sensitive.

We showed that in the case of no P-gp transfer the sensitive cells dominate and now, with fully optimized parameters capturing the experimental data, we see that the transfer of resistance cannot affect the system enough to overcome the inherent competitive advantage of the sensitive cells. In the next section we incorporate a drug in order to study the effects of chemotherapy on sensitive cells, resistant cells, and the tumor as a whole.

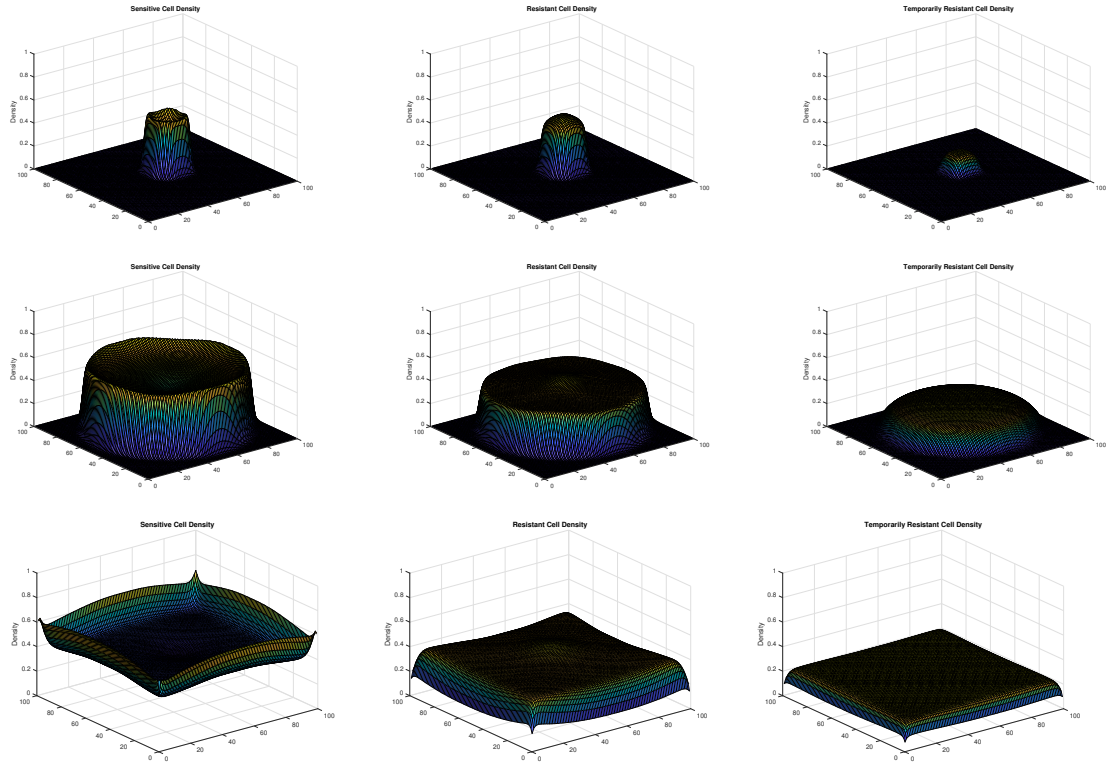

Figure 4.6: Simulation of (4.7) over 100 hours. Densities of sensitive (left), resistant (middle), and temporarily resistant (right) cells are plotted over time. Top: t=10 hours. Middle: t=50 hours. Bottom: t=100 hours.

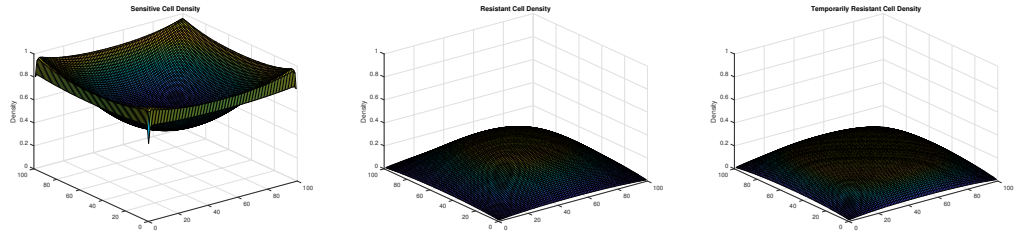

Figure 4.7: Simulation of (4.7) over two months. Densities of sensitive (left), resistant (middle), and temporarily resistant (right) cells are plotted over time.

4.3 Drug Treatment

We now take a sideways step and remove the temporarily resistant cells in order to study how a cytotoxic drug affects the system with solely sensitive and resistant cells. We allow the drug to affect both sensitive and resistant cells, as the overexpression of P-gp does not make a cell immune to the drug. The new model is written as:

$$\frac{\partial u}{\partial t} = D_u \Delta u + u(1-u-v) - d_u uc, \tag{4.8a}$$

$$\frac{\partial v}{\partial t} = D_v \Delta v + av(1-u-v) - d_v vc, \tag{4.8b}$$

$$\frac{\partial c}{\partial t} = \nabla \cdot (D(v) \nabla c) - c(\gamma + \lambda_u u + \lambda_v v). \tag{4.8c}$$

The drug, c, shrinks both the sensitive and resistant cell populations through a mass action term, where $d_u >> d_v$ to represent the inherent resistance in v. The diffusion of the drug is affected by the term $D(v)$. The overexpression of P-gp in the resistant cells expels the drug so we will have $\frac{\partial D}{\partial v} > 0$, signifying an increase in diffusion when the drug is in the presence of resistant cells. In this section we set $D(u, v) = 1 + \epsilon v^2$ for a small $\epsilon > 0$. The final term represents the accumulation of decay and uptake loss of the drug. $\gamma < 1$ is the fraction of the drug that decays at each time step. λ_u and λ_v are parameters that mediate the amount of drug that is ingested by sensitive and resistant cells, respectively. Since the overexpression of P-gp pumps allows resistant cells to push the drug back out, $\lambda_v < \lambda_u$.

4.3.1 Simulations of The Drug Treatment Model (4.8)

We begin with two simulations of the system (4.8) under constant infusion of the drug. $c = 5$ is the continuous boundary condition in Figures 4.8 & 4.9. Both figures show the development of sensitive and resistant cells over a time scale of 500 hours. Now that we are using the optimal parameters we study the effects of a drug past several days. We see that the number of sensitive cells is dramatically reduced, understandably so with $d_u = 0.85$ and $d_v = 0.2$. We do not allow resistant cells to be completely resistant, allowing some of the drug to get past the volume of P-gp pumps. It is clear that continuing this further will result in the resistant cells completely taking over, rendering chemotherapy ineffective. Figure 4.8 shows the results of initial 1:1 ratio in the same location in the center of the domain, while Figure 4.9 shows the dynamics if the tumor were split into two distinct regions, one filled with sensitive cells and the other solely resistant. The results after 500 hours are almost indistinguishable, suggesting the physical makeup of the tumor does not play a role in the overtaking by the resistant cells.

Figure 4.10 shows the same development of the system but under a significantly smaller drug dose. In this case $c = 0.1$ on the boundary and so the effects of the drug are notably slowed. The middle two plots, showing the system after 100 hours, or approximately 3 days, demonstrates that the competitive advantage of the sensitive cells is still active in the middle region. The drug has not yet managed to penetrate deep into the tumor and so there are more sensitive cells there. Meanwhile near the boundary, the sensitive cells have been eliminated and that is where the resistant

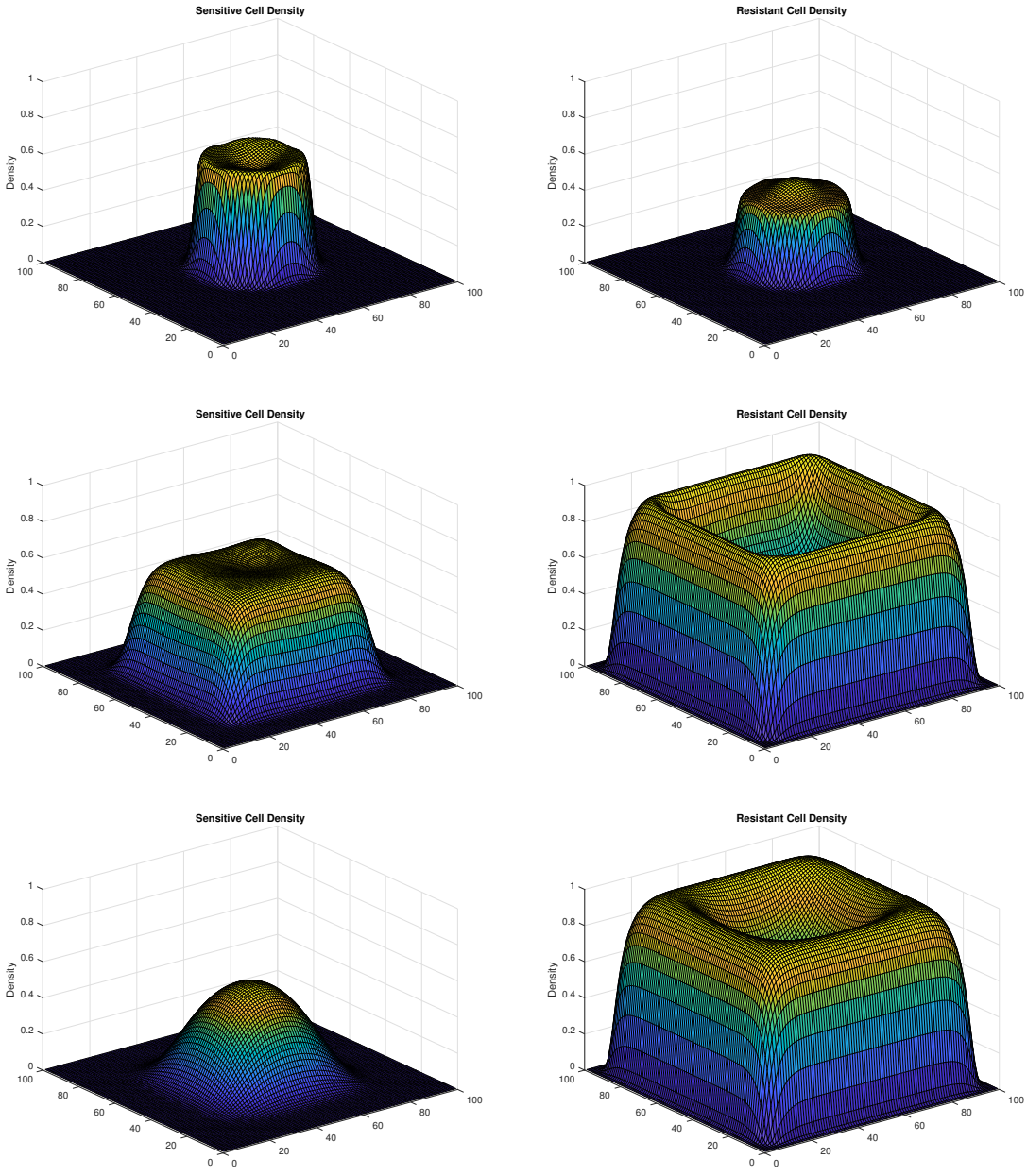

Figure 4.8: Simulation of (4.8). Initial centered 1:1 ratio. Densities of sensitive (left) and resistant (right) cells are shown over time under constant drug infusion (c=5). Top: t=20 hours. Middle: t=100 hours. Bottom: t=500 hours.

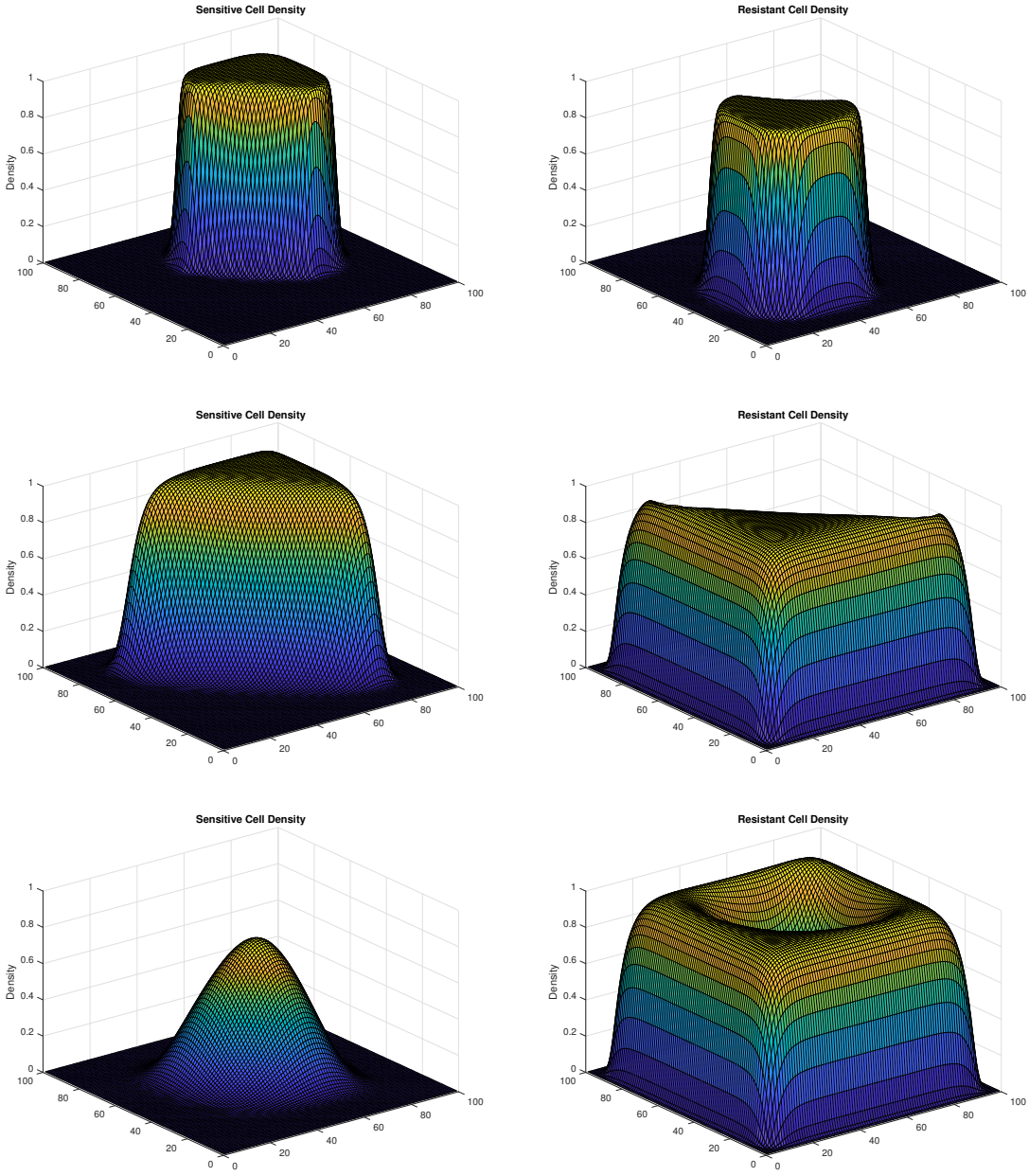

Figure 4.9: Simulation of (4.8). Initial 1:1 ratio, separated into distinct sections of only sensitive and only resistant cells. Densities of sensitive (left) and resistant (right) cells are shown over time under constant drug infusion (c=5). Top: t=20 hours. Middle: t=100 hours. Bottom: t=500 hours.

cells are growing more rapidly.

The most important result is shown in Figures 4.11 and 4.12. Under uniform constant infusion of a drug on the boundary, we are unable to prevent the tumor from growing. As seen in Figures 4.8 and 4.9, constant infusion eradicates the sensitive cells and leaves a resistant tumor growing with little inhibition. Even in the case of a small dose, the resistant population will eventually take over and the therapy will be unsuccessful.

4.4 The Full Model

We combine all ingredients together in our full model. This model incorporates the transfer of P-gp pumps as well as a chemotherapeutic agent. All populations: sensitive (4.9a), resistant (4.9b, and temporarily resistant (4.9c), have now has a mass action death term due to interaction with the drug. A new uptake term $\lambda_w w$ is included in the equation for the drug. The diffusion coefficient $D(v)$ is now $D(v,w)$, with $\frac{\partial D}{\partial v} > 0$ and $\frac{\partial D}{\partial w} > 0$, and we take it to be $D(v,w) = 1 + \epsilon(v+w)^2$. The resulting system is:

$$\frac{\partial u}{\partial t} = D_u \Delta u + u(1-u-v-w) - k_u uv + k_w w - d_u uc, \tag{4.9a}$$

$$\frac{\partial v}{\partial t} = D_v \Delta v + a_v v(1-u-v-w) - d_v vc, \tag{4.9b}$$

$$\frac{\partial w}{\partial t} = D_w \Delta w + a_w w(1-u-v-w) + k_u uv - k_w w - d_w wc, \tag{4.9c}$$

$$\frac{\partial c}{\partial t} = \nabla \cdot (D(v,w) \nabla c) - c(\gamma + \lambda_u u + \lambda_v v + \lambda_w w). \tag{4.9d}$$

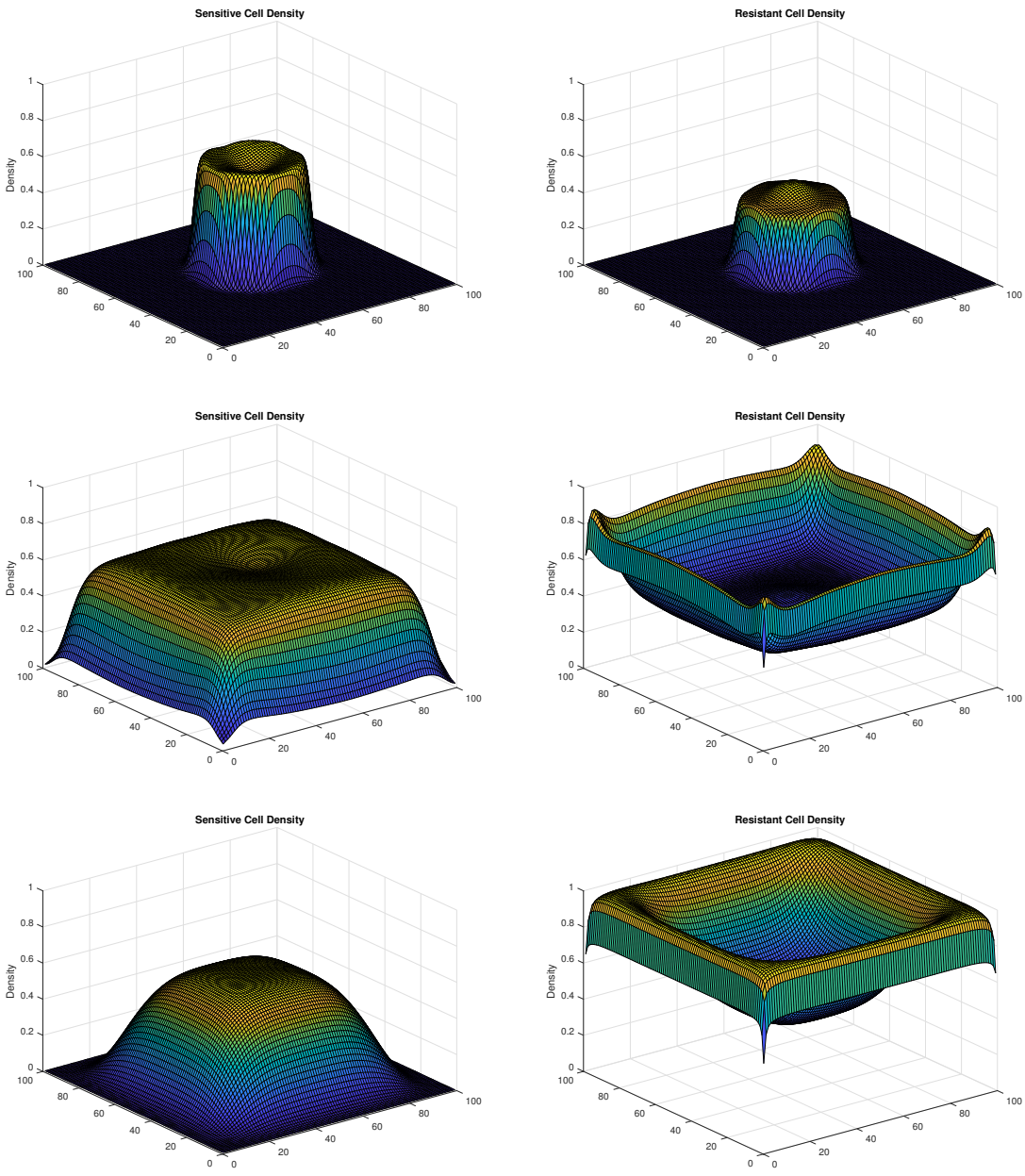

Figure 4.10: Simulation of (4.8). Densities of sensitive (left) and resistant (right) cells are shown over time under constant drug infusion (c=0.1). Top: t=20 hours. Middle: t=100 hours. Bottom: t=500 hours.

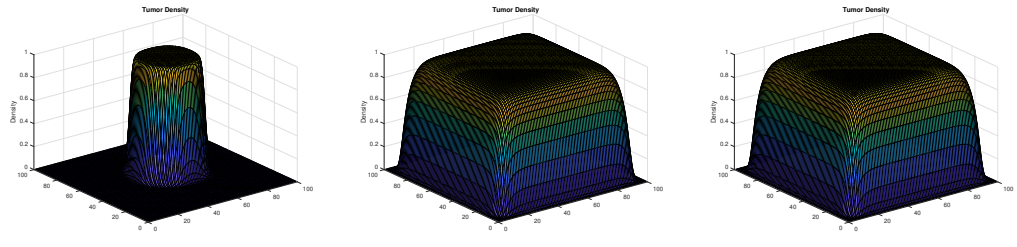

Figure 4.11: Simulation of (4.8). Overall tumor density is shown over a period of 100 hours under constant drug infusion (c=5). Left: t=20 hours. Middle: t=100 hours. Right: t=500 hours.

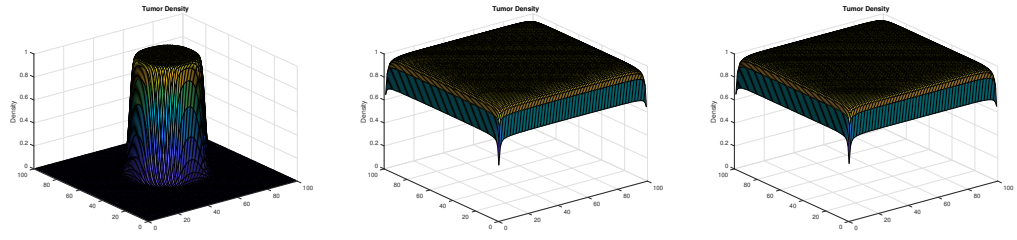

Figure 4.12: Simulation of (4.8). Overall tumor density is shown over a period of 100 hours under constant drug infusion (c=5). Left: t=20 hours. Middle: t=100 hours. Right: t=500 hours.

We use the complete model to study the effects of varying therapy protocols. We run simulations for constant infusion, intermittent infusions, and a combination of the two. We also find drug protocols that minimize overall tumor size and also total density of resistant cells.

4.4.1 Constant Infusion

We previously saw that a constant infusion of the drug would force the sensitive population to contract until the system is dominated by resistant cells. Since the only change is a new mechanism (transfer of resistance) that diminishes the sensitive cell population, it makes sense that the full model will induce similar dynamics. In this case not only is the drug coming in from the boundary harming the sensitive cells but so does the interaction with the initial resistant cells in the center. This is shown in Figure 4.13, with $c = 5$ on the boundary. The temporarily resistant cells emerge in the center of the domain, where there is an overlap between resistant and sensitive cells. This population continues to grow until the population of sensitive cells is so small that there are not enough cells left to sustain the size of the temporarily resistant population. Figure 4.14 shows the same time frame but with a smaller dose ($c = 0.1$) along the boundary. Again, the resistant cell population grows faster near the boundary while the sensitive population decreases in the center due to the transfer of P-gp pumps. Both cases show what we have previously seen: a constant infusion of a drug does very little to limit the growth of the resistant cell population.

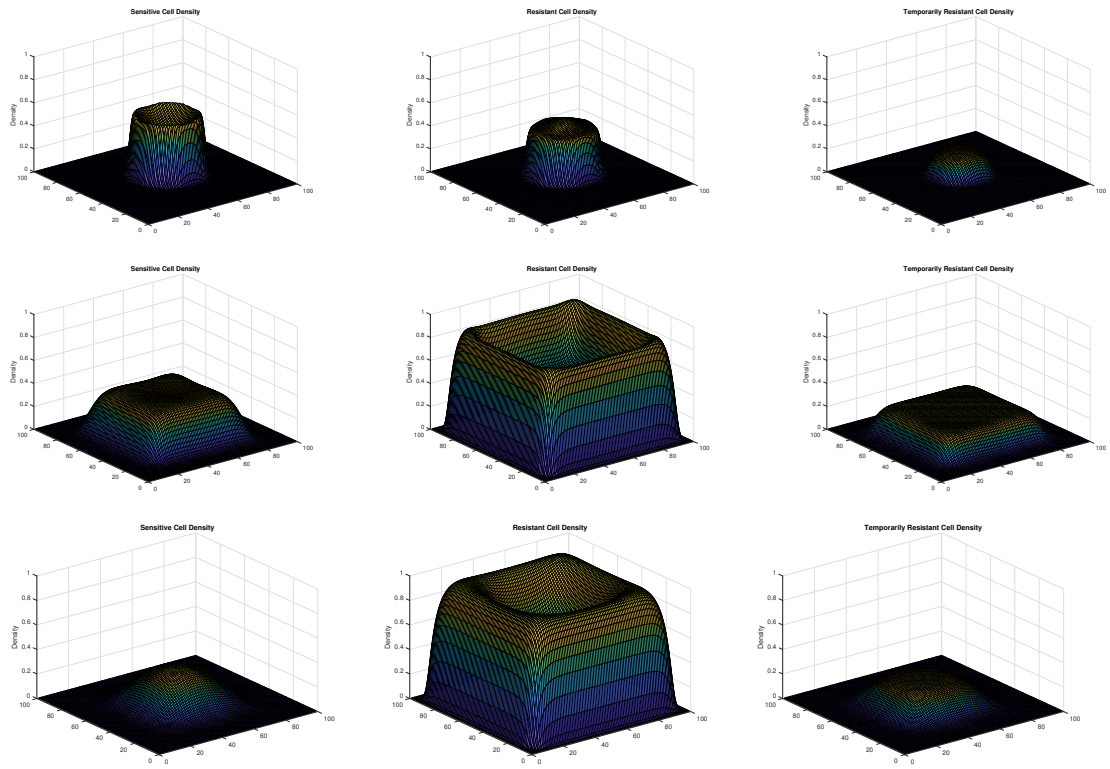

Figure 4.13: Simulation of (4.9) with initial 1:1 ratio. Densities of sensitive (left), resistant (middle), and temporarily resistant (right) cells are shown over time under constant drug infusion (c=5). Top: t=20 hours. Middle: t=100 hours. Bottom: t=500 hours.

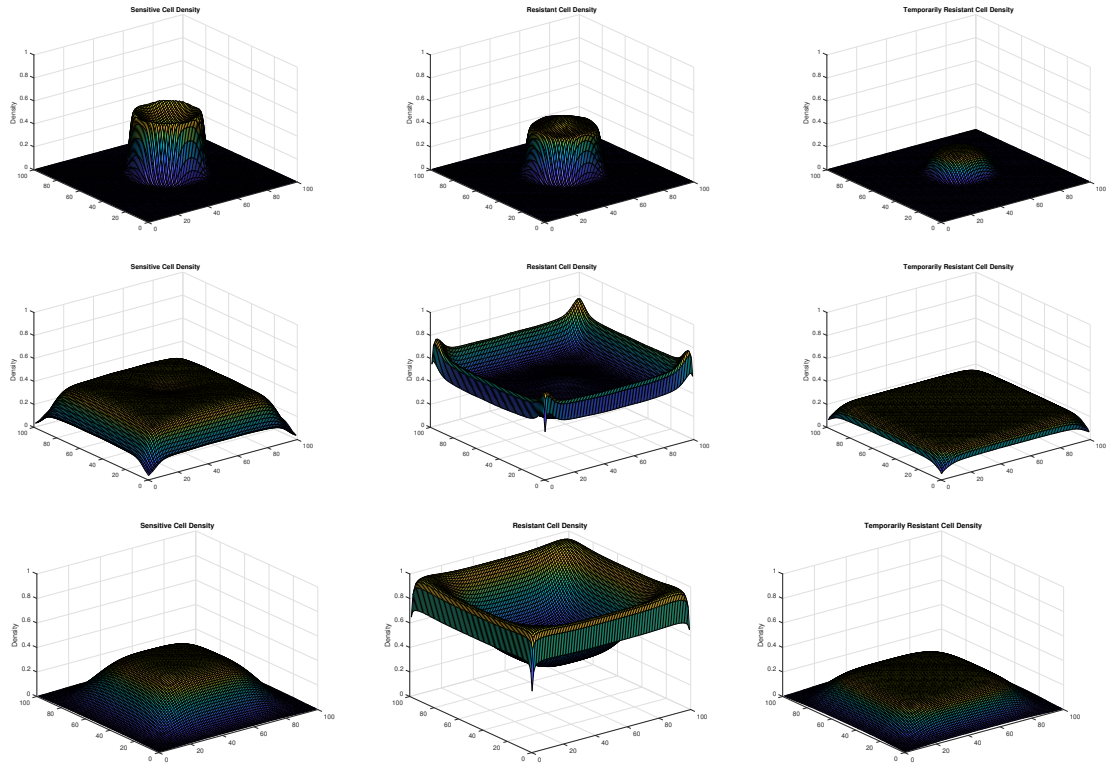

Figure 4.14: Simulation of (4.9) with initial 1:1 ratio. Densities of sensitive (left), resistant (middle), and temporarily resistant (right) cells are shown over time under constant drug infusion (c=0.1). Top: t=20 hours. Middle: t=100 hours. Bottom: t=500 hours.

4.4.2 On-Off Therapy

Since constant drug infusion will eliminate all sensitive cells and lead to a drug resistant tumor, we consider other treatment protocols. We need to maintain a robust sensitive cell population since that is the only mechanism for controlling the resistant population. We study this scenario in a series of simulations. In each simulation we administer the drug for 8 hours at a time and then turn it off for varying lengths of time. Figures 4.15 and 4.16 show the results over 500 hours of implementing the treatment every 24 hours. In this case it is 8 hours on and 16 hours off. Figure 4.15 is for the higher dose, $c = 5$, while Figure 4.16 shows the effects of the lower does, $c = 0.1$. We see in Figure 4.15 that we still have a significant upswell in the resistant population and a resistant cell-dominated tumor develops within days. The smaller dose, on the other hand, allows the sensitive population to control the growth of resistant cells.

Figures 4.17 & 4.18 show the same two scenarios but with the drug administered once every 96 hours rather than once a day. We see again that the lower dose allows the sensitive cells to sustain themselves. In between doses, the sensitive cells grow along the boundary where resistant cells are at their lowest levels.

With the simulations as a guide we consider optimizing therapy protocols to minimize the overall size of the tumor and separately to minimize the number of resistant cells present.

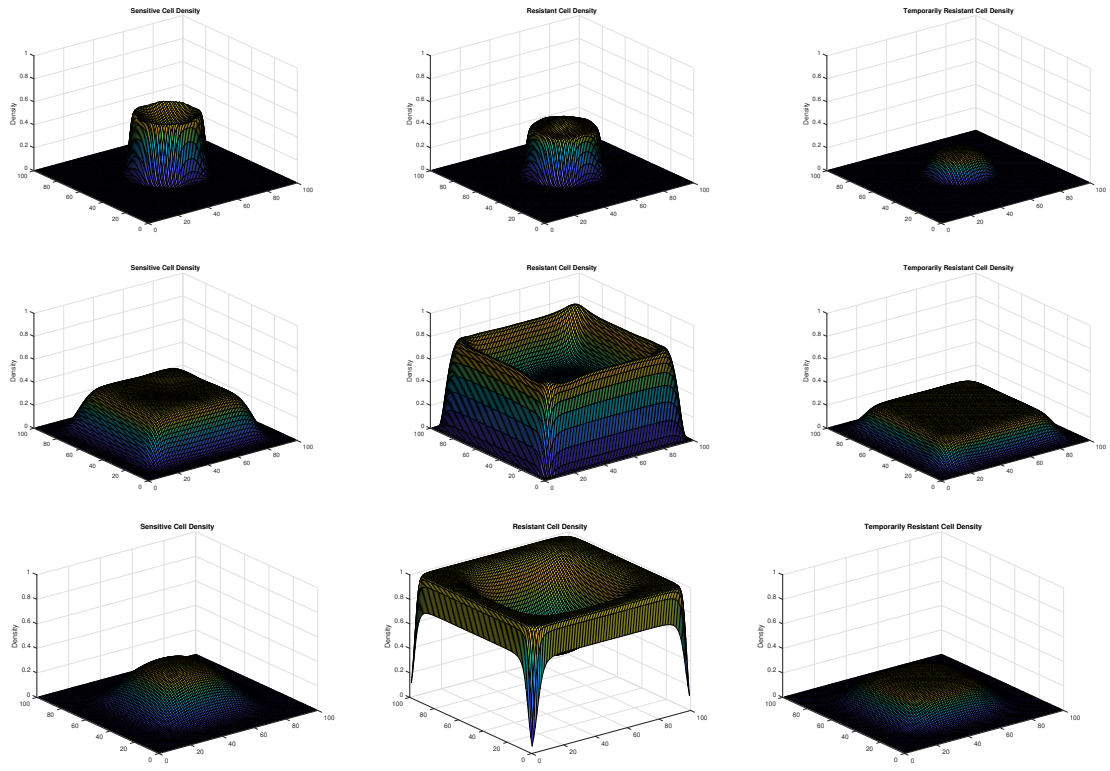

Figure 4.15: Simulation of (4.9) with initial 1:1 ratio. Densities of sensitive (left), resistant (middle), and temporarily resistant (right) cells are shown over time under on/off therapy (c=5). The drug is pumped for 8 hours at a time every 24 hours. Top: t=20 hours. Middle: t=100 hours. Bottom: t=500 hours.

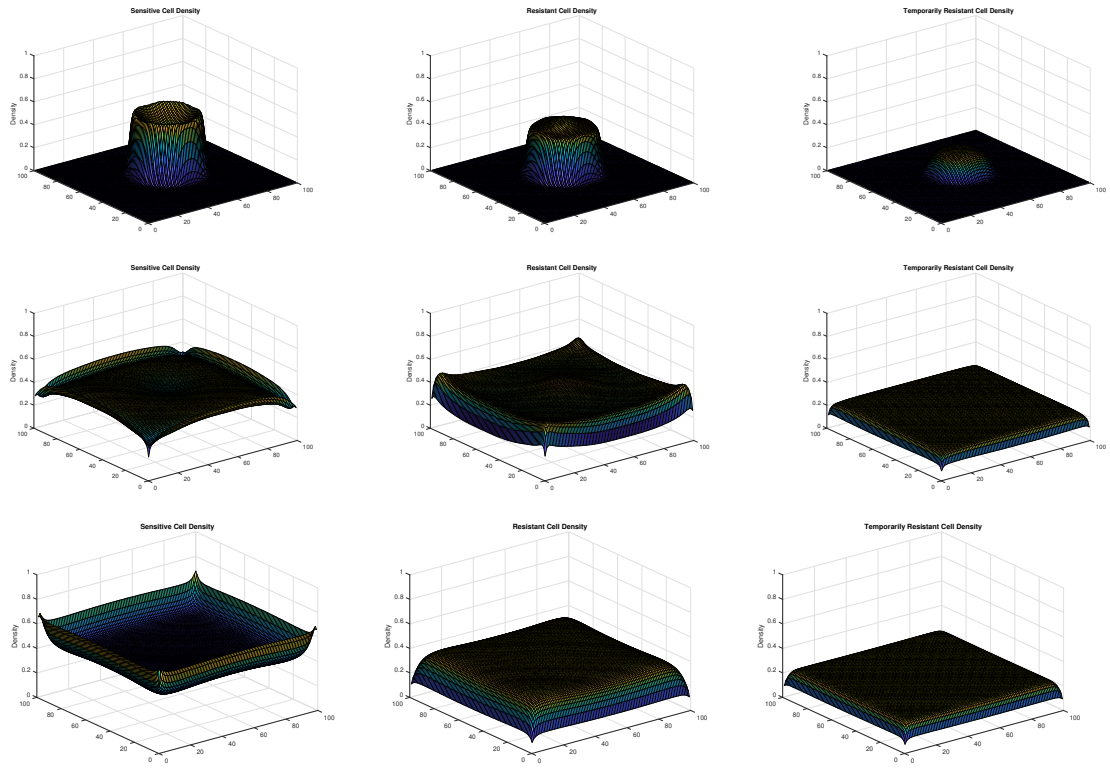

Figure 4.16: Simulation of (4.9) with initial 1:1 ratio. Densities of sensitive (left), resistant (middle), and temporarily resistant (right) cells are shown over time under on/off therapy (c=0.1). The drug is pumped for 8 hours at a time every 24 hours. Top: t=20 hours. Middle: t=100 hours. Bottom: t=500 hours.

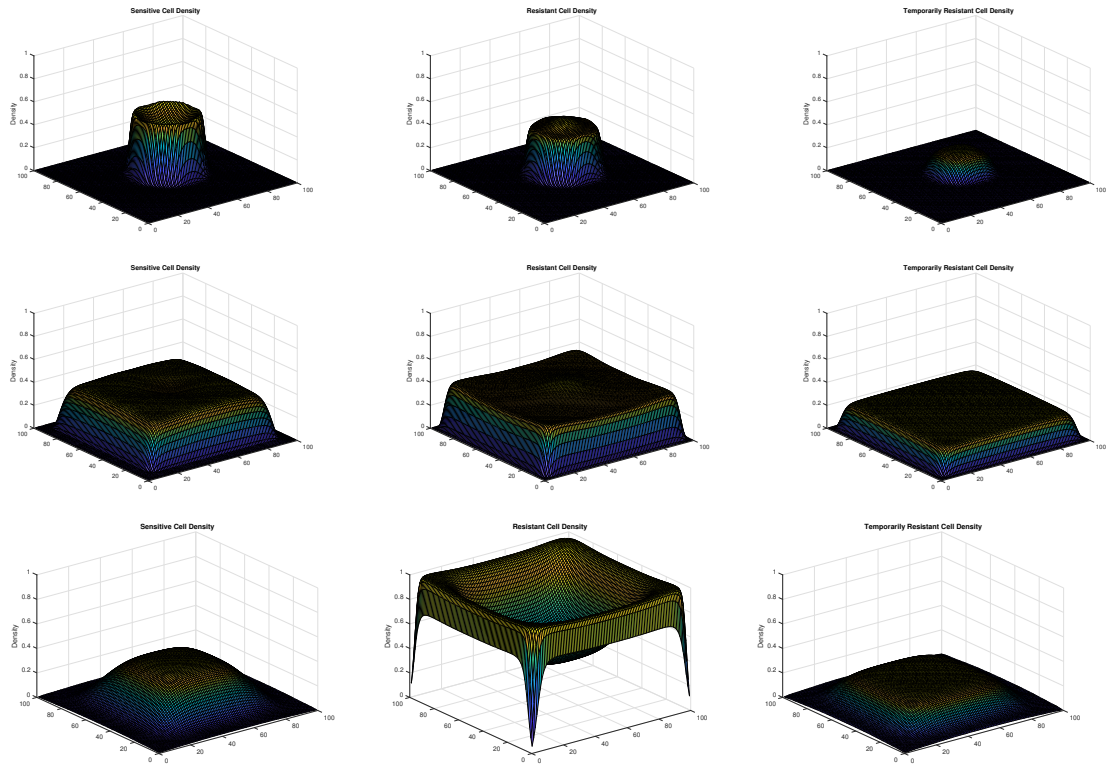

Figure 4.17: Simulation of (4.9) with initial 1:1 ratio. Densities of sensitive (left), resistant (middle), and temporarily resistant (right) cells are shown over time under on/off therapy (c=5). The drug is pumped for 8 hours at a time every 96 hours. Top: t=20 hours. Middle: t=100 hours. Bottom: t=500 hours.

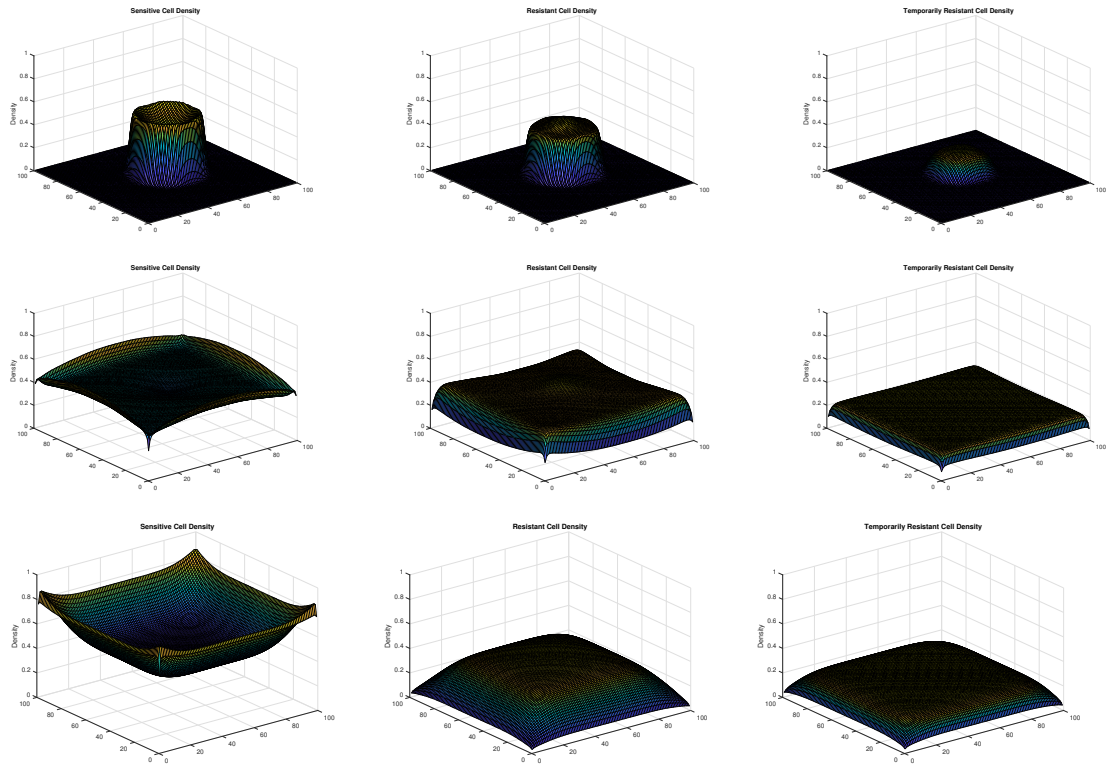

Figure 4.18: Simulation of (4.9) with initial 1:1 ratio. Densities of sensitive (left), resistant (middle), and temporarily resistant (right) cells are shown over time under on/off therapy (c=0.1). The drug is pumped for 8 hours at a time every 96 hours. Top: t=20 hours. Middle: t=100 hours. Bottom: t=500 hours.

4.4.3 Optimal Therapies

In order to find an optimal treatment plan we first consider minimizing the size of the tumor. We do this in two separate ways. First, we look at the functional

$$J = \int_0^{t_{end}} (u^m + v^m + w^m)\, dt, \tag{4.10}$$

where $J(u, v, w, c, t)$ is the total volume of the tumor over the entire simulation, and m is either 1 or 2, for linear or quadratic control. We also consider $K = u(t_{end}) + v(t_{end}) + w(t_{end})$ for a measure of the size of the tumor at the end of the simulation. Since we do not need to look at every single possible treatment plan, we pick 11 protocols, ranging from constant infusion to infusion once every three weeks. We also allow for 8 different sizes of the dose, ranging from no drug, c=0, to c=100. In finding the optimal treatment plan for these options we see that the treatment that minimizes the total volume of the tumor J is the same as the treatment that minimizes the final volume of the tumor K. Unfortunately, this optimal result is constant infusion with the highest dose possible. We have already seen that constant infusion leads to a sharp increase in the proportion of resistant cells and allows them to eventually take over and dominate.

With that result we then look at what treatment plan will minimize the amount of resistant cells in the tumor. As long as we can keep the resistant cell population low then there is an opportunity for chemotherapy to work. We optimize over the same set and the result is the opposite approach from the one we found above. As the previous simulations suggested, the lower the drug dose, the better the chance

that the sensitive cells would control the resistant population. We find that the way to minimize resistant cells is, in fact, to deliver no drug at all. This makes sense in our model since, with d_v and d_w so small, the one truly effective mechanism for keeping the resistant cell population down is the competitive advantage of the sensitive cells. Any drug input decreases their number significantly and so the optimal way to control the resistant population is to leave the sensitive population uninhibited, meaning no chemotherapy at all.

4.5 Discussion

In this chapter we presented a model of P-gp transfer in a two-dimensional space. We began with a simple reaction-diffusion system and incorporated the transfer of resistance as well as chemotherapeutic agent. When $a < 1$, the competitive advantage allows the sensitive cells allows them to grow at the expense of the resistant population. While the spread of temporary resistance through the transfer of P-gp pumps does not have a strong enough effect to overcome this trend on its own, the inclusion of a drug may result with a significant growth of the resistant population.

In looking for optimal treatment protocols we run into a conundrum. The resistant population is minimized when no drug is applied, yet this leads to the maximum tumor size. The tumor size is minimized when treated with a constant infusion of a large dose, yet this leads to an almost fully resistant tumor. Higher amounts of drug result with smaller tumors. Unfortunately, this correlates with the

emergence of more resistant tumors. Within the confines of this model we cannot achieve a treatment protocol that slows down tumor growth while also assuring that tumor does not become resistant over time.

Chapter 5: A Model for Drug Resistance as a Continuous Variable

5.1 Introduction

In this chapter we extend the work by Pasquier *et. al.* [44], and the latest paper, Magal *et. al.* [3], from the same group. These studies treat resistance as a continuous variable. Magal *et. al.* [3] consider a PDE model with a Boltzmann type integral describing the transfer of P-gp under multiple transfer rules:

$$\frac{\partial u(t,x)}{\partial t} = 2\tau[T(u(t,\cdot))(x) - u(t,x)], \text{ for } x \in \mathbb{R} \tag{5.1a}$$

$$u(0,\cdot) = u_0 \in L^1_+(\mathbb{R}). \tag{5.1b}$$

Here $u(t,x)$ is the density of cancer cells at time t with resistance level x, defined between 0 and 1. The transfer operator T, is defined as:

$$T(u)(x) = \begin{cases} \frac{\hat{T}(u)(x)}{\int_{\mathbb{R}} u(r)\mathrm{d}r} & \text{if } \int_{\mathbb{R}} u(r)\mathrm{d}r \neq 0, \\ 0 & \text{otherwise,} \end{cases} \tag{5.2}$$

where

$$\begin{aligned} \hat{T}(u)(x) \coloneqq & \int_{\mathbb{R}} \pi_1(p)u(x + f_1(p)p)u(x - (1 - f_1(p)p)\mathrm{d}p \\ & + \int_{\mathbb{R}} \pi_2(p)u(x + f_2(p)p)u(x - (1 - f_2(p)p)\mathrm{d}p. \end{aligned} \tag{5.3}$$

The model exhibits an intrinsic death term along with T, a growth rate due to a transfer of P-gp between individual cells. The probability that a pair of cells

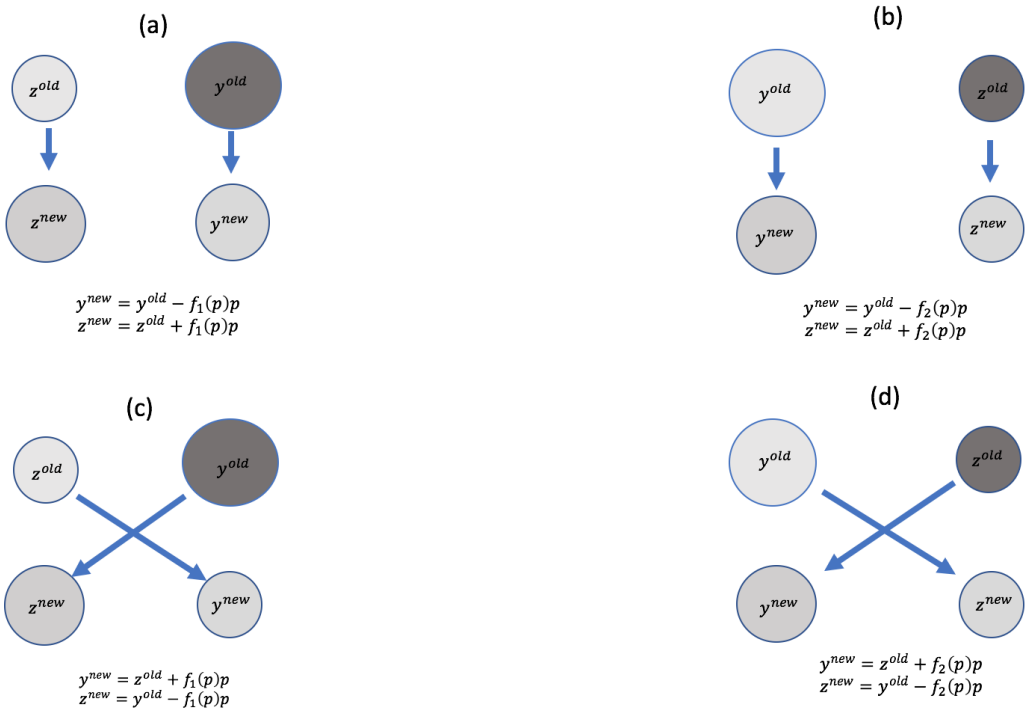

Figure 5.1: The possible transfers under each transfer efficiency f_1 and f_2. y^{old} and z^{old} are the transferrable quantities of P-gp expression. $y^{old} > z^{old}$ in all four scenarios. Figure adapted from [3].

is involved in a transfer is chosen randomly and is independent of resistance levels. τ represents the transfer rate where the time between transfers is modeled by an exponential law with mean τ^{-1}. $f(p)$ is the transfer efficiency and each cell has an intrinsic p value and those with higher p values lose $f(p)$ times the difference of the p values of the two cells involved in the transfer. In [44] only one transfer efficiency function $f(p)$ is used, while in [3] two different efficiency functions, f_1 and f_2, are considered with the probability of each written as:

$$\pi_1(p) = \frac{[\frac{1}{2} - f_2(p)]}{[1 - (f_1 + f_2)(p)]} \qquad \text{and} \qquad \pi_2(p) = \frac{[\frac{1}{2} - f_1(p)]}{[1 - (f_1 + f_2)(p)]}. \tag{5.4}$$

Figure 5.1 shows the four different types of transfer functions with efficiencies $f_1(p)$ and $f_2(p)$. There are four possible transfers resulting in resistance level y^{new} and four corresponding transfers resulting in z^{new}. The new resistance level y^{new} can come from y^{old} giving away $f_1(p)p$ or $f_2(p)p$ of its resistance level to lower it to y^{new} as seen in Figure 5.1(a) and 5.1(b). Alternately, y^{new} can come from z^{old} gaining either $f_1(p)p$ or $f_2(p)p$ to increase its resistance level.

We extend this idea to include cellular proliferation as well as a new spatial dimension. In Section 5.2 we introduce our model with a single transfer rule and discuss simulations and results. In Section 5.3 we add a cytotoxic drug and study its effect on the distribution of resistance levels. In Section 5.4 we extend the work to include two transfer rules f_1 and f_2. Concluding remarks are provided in Section 5.5.

5.2 The First Model

We incorporate the idea of continuous resistance into a reaction-diffusion model. We develop a model that includes the transfer of resistance alongside diffusion and density inhibited population growth. We denote p as the continuous resistance variable, and x as the 2-dimensional space variable. Each cell occupies a location (i, j) in the 2-d domain. We keep the assumptions on P-gp transfer from [3]. The addition in the transfer term is the stipulation that cells must be within a small neighborhood of each other to be able to transfer P-gp. The model is shown below:

$$\frac{\partial u(x,p,t)}{\partial t} = D\Delta u + au(1-u) + 2\tau\Big[\int_{\mathbb{B}(x)} T(u)(p)\,dx - u\Big] \tag{5.5a}$$

$$u(\cdot,\cdot,0) = u_0 \in L^1_+(\mathbb{R}). \tag{5.5b}$$

We set Dirichlet boundary conditions with $u(0,\cdot,\cdot) = u(X,\cdot,\cdot) = 0$. D is the diffusion coefficient and a controls the speed of cellular growth. $2\tau\int_{\mathbb{B}(x)} T(u)(p)\,dx$ describes all the cells that have resistance level p after a successful transfer. $-2\tau u$ is the flux representing cells that had resistance level p but have successfully transferred P-gp. τ is the rate of P-gp transfer per unit of time.

We develop a transfer term with a single transfer rule based on [80]. We integrate over a small neighborhood allowing the cancer cells to only transfer resistance

to others nearby. The transfer term $T(u)(p)$ is written as:

$$T(u)(p) = \begin{cases} \frac{\hat{T}(u)(p)}{\int_{\mathbb{R}} u(x)\mathrm{d}x} & \text{if } \int_{\mathbb{R}} u(x)\mathrm{d}x \neq 0, \\ 0 & \text{otherwise.} \end{cases} \tag{5.6}$$

$\hat{T}(u)(p)$ follows the scenarios in Figure 5.2 and is of the form:

$$\hat{T}(u)(p) := \int u\left(\frac{p - p_2 f}{1-f}\right) u(p_2) dp_2 + \int u\left(\frac{p-(1-f)p_2}{f}\right) u(p_2) dp_2. \tag{5.7}$$

Here, $f(p) \equiv f$ is the transfer efficiency, defined as a constant. We incorporate the idea from [3] that interaction between cells with a large and a small difference in resistance level should not yield large changes. We define f as follows:

$$f(p_1 - p_2) = \begin{cases} f & \text{if } (p_1 - p_2) \in (\delta_{min}, \delta_{max}), \\ \epsilon_f f & \text{otherwise.} \end{cases} \tag{5.8}$$

Here, f is a function of the difference in resistance levels p_1 and p_2. If the resistance levels of the two interacting cells are within a threshold then the transfer efficiency is f. If they are too small or too large, the transfer efficiency becomes $\epsilon_f f$, for a small $\epsilon_f > 0$. The amount of P-gp transferred is determined by multiplying the densities of the two transferring entities. The explanation for the terms inside the integrals follows below.

Figure 5.2 shows the four possible scenarios in which a cell results in resistance level p after a transfer. Assume two cells have resistance levels p_1 and p_2. If $p_1 \leq p_2$ then their interaction will lead to p_2 transferring a certain amount of resistance to p_1. There are two ways that can end in a cell with resistance level p. (i): if

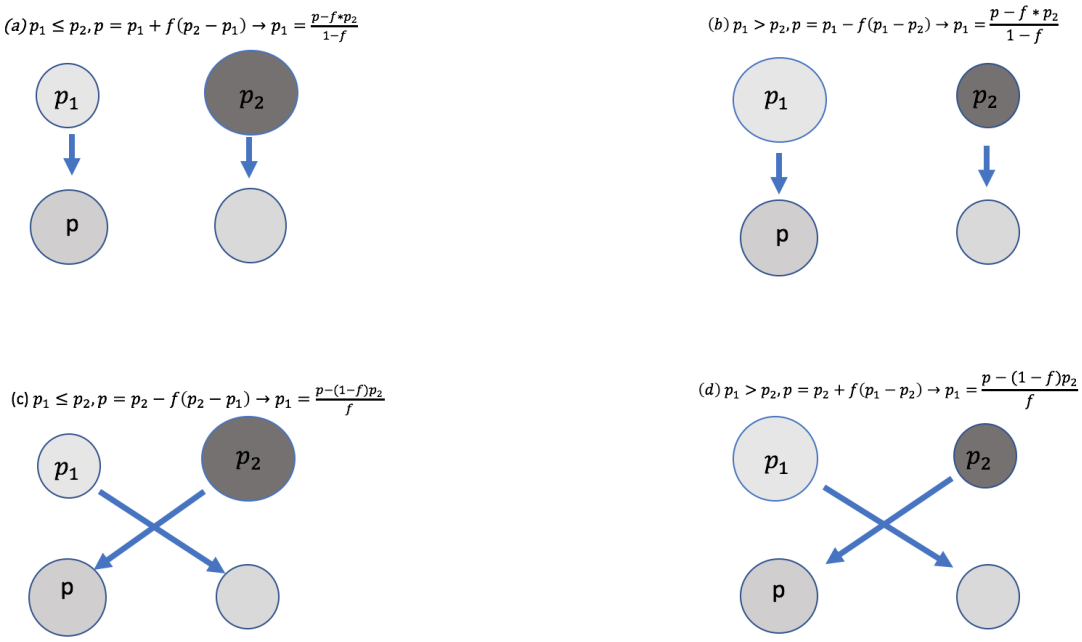

Figure 5.2: The four possible transfers resulting in a cell having P-gp expression level p with one predecessor having P-gp expression level p_2. Figure adapted from [80].

$p = p_1 + f * (p_2 - p_1)$ then we solve for p_1 so $p_1 = \frac{p - fp_2}{1-f}$. (ii): if $p = p_2 - f * (p_2 - p_1)$ then we solve for p_1 so $p_1 = \frac{p-(1-f)p_2}{f}$. Now, if $p_2 \leq p_1$ we have the two scenarios but with the two cells in the opposite position: (i): if $p = p_1 - f * (p_1 - p_2)$ then we solve for p_1 so $p_1 = \frac{p - fp_2}{1-f}$. (ii): if $p = p_2 + f * (p_1 - p_2)$ then we solve for p_1 so $p_1 = \frac{p-(1-f)p_2}{f}$. Despite having four scenarios there is overlap so we only have two distinct values for p_1 in terms of the desired resistance level p and any other resistance level p_2. This gives us the two integral terms in (5.7).

The continuous model has two qualitative changes from the model in Chapter 4. In this setting we do not consider temporary levels of resistance. Each transfer is considered a permanent change. We also assume that resistance cells lose a portion of their resistance during each transfer, unlike (4.9). In Chapter 4 P-gp transfer is assumed to affect only sensitive cells.

5.2.1 Numerical Methods

We discretize our model (5.5)-(5.8) in a similar manner to section 4.1.1. We use a semi-explicit method of updating each component, with explicit Euler discretization in time, and our implicit 5-point stencil in space. We repeat the specifics below, with the addition of an extra dimension p.

We use n for each time step and i and j for the two spatial dimensions. The time derivatives are discretized via the forward, or explicit, Euler method, with $k = \Delta t$:

$$\frac{\partial u}{\partial t}|_{t=n} \approx \frac{u^{n+1}_{i,j,p} - u^{n}_{i,j,p}}{k}. \tag{5.9}$$

We use an implicit 5-point stencil for the finite difference approximations. In this case the (i, j) component of the Laplacian at time step n is written as

$$\Delta u \approx \frac{u^{n+1}_{i+1,j,p} + u^{n+1}_{i-1,j,p} + u^{n+1}_{i,j+1,p} + u^{n+1}_{i,j-1,p} - 4u^{n+1}_{i,j,p}}{h^2}, \tag{5.10}$$

where $h = \Delta x$. For each $u^{n+1}_{i,j,p}$, we have:

$$\begin{aligned} u^{n+1}_{i,j,p} \approx D_u \lambda \left(u^{n+1}_{i+1,j,p} + u^{n+1}_{i-1,j,p} + u^{n+1}_{i,j+1,p} + u^{n+1}_{i,j-1,p} - 4u^{n+1}_{i,j,p}\right) \\ + a u^n_{i,j,p}(1 - u^n_{i,j,p})k + 2\tau(F - u^n_{i,j,p})k + u^n_{i,j,p}, \end{aligned} \tag{5.11}$$

with F defined in (5.12) and $\lambda = \frac{k}{h^2}$. We solve the linear system (5.11) in Matlab utilizing the efficiency of sparse matrices. The simulations of the extensions of this model used in the upcoming sections all use a similar discretization.

Our spatial grid is coarse enough that we allow cancer cells to transfer P-gp to others within the same grid space. If both cells are of the form $u(i, j, :)$ they have an interaction and transfer the protein between each other. F is the discretization at time $t = n$ of the transfer term (5.6)-(5.7).

$$F = \frac{\displaystyle\sum_{P=1}^{Np} u_{(i,j,\frac{p-Pf}{1-f})} u_{(i,j,p)} \Delta p + \sum_{P=1}^{Np} u_{(i,j,\frac{p-(1-f)P}{f})} u_{(i,j,p)} \Delta p}{\displaystyle\sum_{i=1}^{N}\sum_{j=1}^{N}\sum_{m=1}^{Nm} u_{i,j,p} \Delta p * h^2} \tag{5.12}$$

The parameters used in the simulations are shown in Table 5.1. We use parameter values from the PDE model in Chapter 4 along with τ and f from [3]. Table 5.2 shows the values used in our simulations.

Table 5.1: Parameter Values & Descriptions

Parameter	Range	Description	Reference
t_{end}	[0,1460] (hours)	Length of Time Interval	Table 4.1
N_z	[10, 1000]	Length of one side of square domain	Table 4.1
dt	[0.1,10] (hours)	Length of discretized time step	Table 4.1
dz	[0.1,10]	Length of spatial step	Table 4.1
D	[0.05,5]	Diffusion coefficient for cancer cells	Table 4.1
a	$[0.5, 5]$	Growth parameter for cancer cells	Table 4.1
τ	[0,1]	Transfer rate of P-gp between cancer cells	[3]
f	[0,1]	Efficiency of transfer of P-gp expression	[3]

Table 5.2: Parameters values used in simulations of (5.5)-(5.7) and (5.13).

Parameter	N_z	N_m	dt	dz	D	D_c
Value	100	100	1	0.5	0.05	1
Parameter	τ	f	ϵ_f	ϵ	a	γ
Value	0.9	0.1	0.01	0.5	0.85	0.4

5.2.2 Simulations

We begin by studying the overall growth of the tumor. Since there is no drug and the transfer of resistance should not affect full tumor growth we expect the simulation to show uninhibited growth up to the carrying capacity.

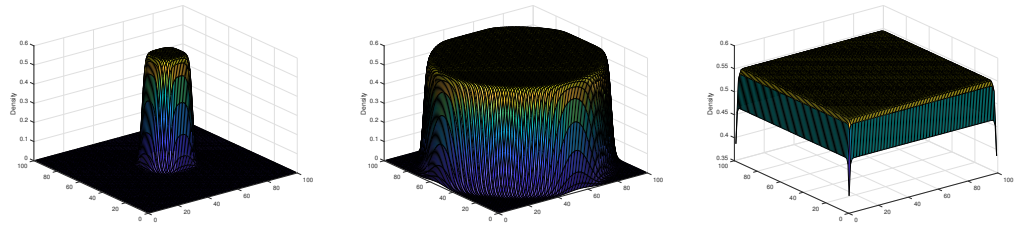

Figure 5.3: Simulation of (5.5)-(5.7). Overall tumor density is shown over a period of 100 hours. Left: t=10 hours. Middle: t=50 hours. Right: t=100 hours.

We see in Figure 5.3 that the tumor grows as expected. We next study the changes in resistance levels. [3] showed that when starting with high amounts of very sensitive and very resistant cells, over a period of 7 days the transfers led to a much more even distribution. To study this setting, we begin with a prescribed initial density for resistance levels between $[0, 0.1]$ and $[0.9, 1]$. We let the density for the population in between be one half of the initial density on each end. Figure 5.4 shows our initial result for a simulation of 100 hours.

We see that very little transfer has taken place. We address this by raising the speed of transfer and simulating for a full week. We see in Figure 5.5 a similarly high level of volatility that was also found in [3]. We also see that after 7 days the resistance level has spread and become more even. This becomes more obvious

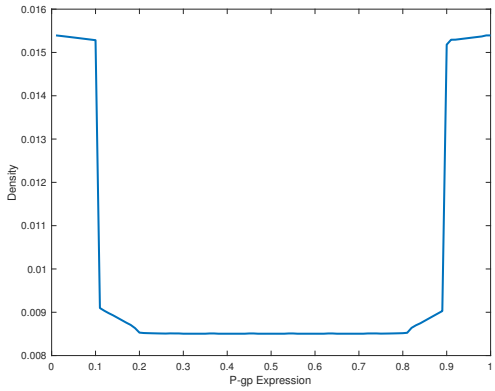

Figure 5.4: Simulation of (5.5)-(5.7) over 100 hours. Density of tumor cells at each level of P-gp expression.

when we zoom out of the far right figure in Figure 5.5, as shown in Figure 5.6.

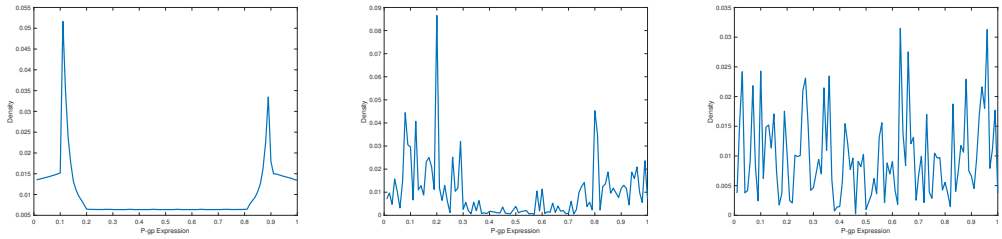

Figure 5.5: Simulation of (5.5)-(5.7). Density of tumor cells at each level of P-gp expression with raised speed of transfer. Left: t=24 hours. Middle: t=96 hours. Right: t=168 hours.

5.3 Incorporating a Drug

We now proceed by including a cytotoxic drug term. We postulate that the drug does not affect the transfer of P-gp so $T(u)(p)$ and $\hat{T}(u)(p)$ remain as in (5.6)

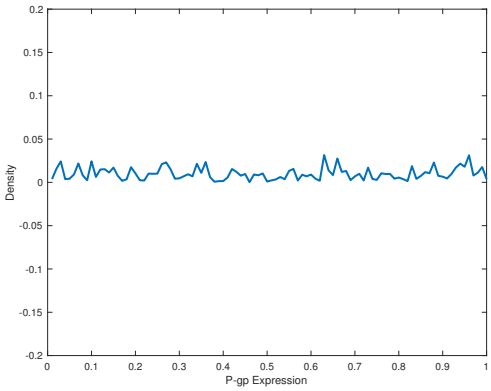

Figure 5.6: Simulation of (5.5)-(5.7) over 168 hours. Density of tumor cells at each level of P-gp expression. Resistance is nearly uniformly distributed in this range.

and (5.7). Our new system is written as:

$$\frac{\partial u(p,x,t)}{\partial t} = D\Delta\, u + a(p)u(1-u) + 2\tau\Big[\int_{\mathbb{B}(x)} T(u)(p)\,dx - u\Big] - d(p)cu, \quad (5.13a)$$

$$\frac{\partial\, c(x,t)}{\partial\, t} = \nabla\cdot(D_c(u)\nabla\, c) - c(\gamma + \lambda_u(p)u). \quad (5.13b)$$

We now set $a = a(p)$ and allow the growth rate of sensitive cells to be marginally faster than those of resistant cells by forcing $\frac{\partial a}{\partial p} < 0$. The drug $c(x,t)$ has a similar setup to (4.8c): It has a natural decay rate γ and its uptake is described by a function $\lambda_u(p)$, allowing for the cells with lower resistance level to absorb more of the drug. The presence of cells with high expressions of P-gp will, as in (4.8c), expel the drug making diffusion slightly faster, thus $\frac{\partial D_c}{\partial p} > 0$. The new term for $u(p,x,t)$ is $-d(p)cu$, a mass action death term due to interaction with the drug. We define $d(p)$ such that $\frac{\partial d}{\partial p} < 0$ so that cells with higher resistance level are less

affected by the drug. We set $d(p) > 0, \forall p$, since even high levels of P-gp expression don't necessarily lead to full MDR.

5.3.1 Simulations of The Drug Treatment Model (5.13)

For each expressed resistance level p we define $a(p)$,$d(p)$, and $\lambda_u(p)$ as follows:

$$a(p) = 0.85 + 0.15(1 - p), \tag{5.14a}$$

$$d(p) = 0.2 + 0.6(1 - p), \tag{5.14b}$$

$$\lambda_u(p) = 0.05 + 0.45(1 - p). \tag{5.14c}$$

Both (5.14a) and (5.14b) are extensions of the values of parameters in (4.8). Maximal resistance corresponds to a death term of $d = 0.2$ and minimal resistance with $d = 0.8$. As in (4.8), the minimal growth term is $a = 0.85$ and fully sensitive cells exhibit growth with $a = 1$. We define $D_c(u) = 1 + \epsilon\, u$ for cells with resistance level 0.5 or higher. $D_c(u) = D_c = 1$ for interaction with cells with resistance level lower than 0.5.

We begin by considering the results of the new definition of $a(p)$ when no drug is present. We use the same initial condition as in Section 5.2.2: a prescribed initial amount of cells with P-gp expression between $[0, 0.1]$ and $[0.9, 1]$ and keep $c = 0$ throughout. We see in Figure 5.7 (left) that the tumor grows to its carrying capacity. More interestingly, Figure 5.7 (right) confirms the dominance of the sensitive cells.

Figure 5.8 shows the results of simulations with varying intensities of a constant drug infusion. The figures on the left show the overall tumor size while the figures on the right show the distribution of resistance levels. We see that as the amount

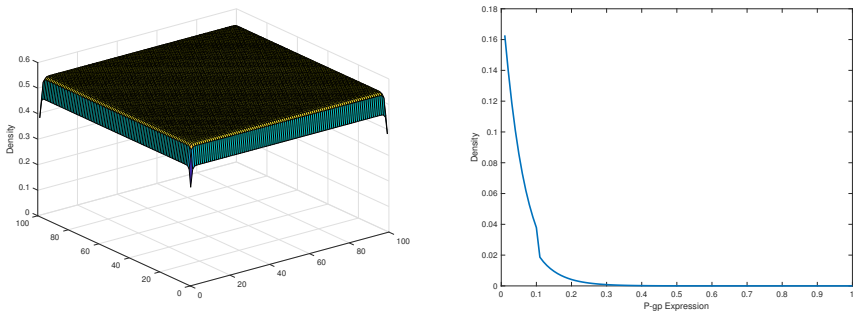

Figure 5.7: Simulation of (5.13) over 100 hours. Left: Overall tumor density. Right: Density of tumor cells at each level of P-gp expression.

of drug is increased, the size of the resistant population grows. The competitive advantage of the cells with less P-gp expression turns out to be strong enough to allow those with the lowest resistance levels to continue to grow despite the presence of the drug. We see this clearer in Figure 5.9 with the spatial layout of the most sensitive and most resistant cells. The left figure shows that the most sensitive cells ($p = 0.01$) are still able to grow near the center of the tumor, while the right figure shows that the most resistant cells ($p = 0.99$) are growing closer to the boundary.

If we allow our initial condition to be an equal amount of cells with each resistance level then we can study the effect of a constant infusion. As seen in Chapter 4, constant infusion should lead to high resistance levels. Figures 5.10 and 5.11 show results of simulations with equal amounts of all resistance levels. Figure 5.10 shows the overall tumor size alongside the distribution along resistance levels. Figure 5.10 (right) is reminiscent of the results in [59], where a constant cytotoxic agent leads to a distribution approaching a delta function centered close to full resistance. We see that the competitive advantage of the most sensitive cells

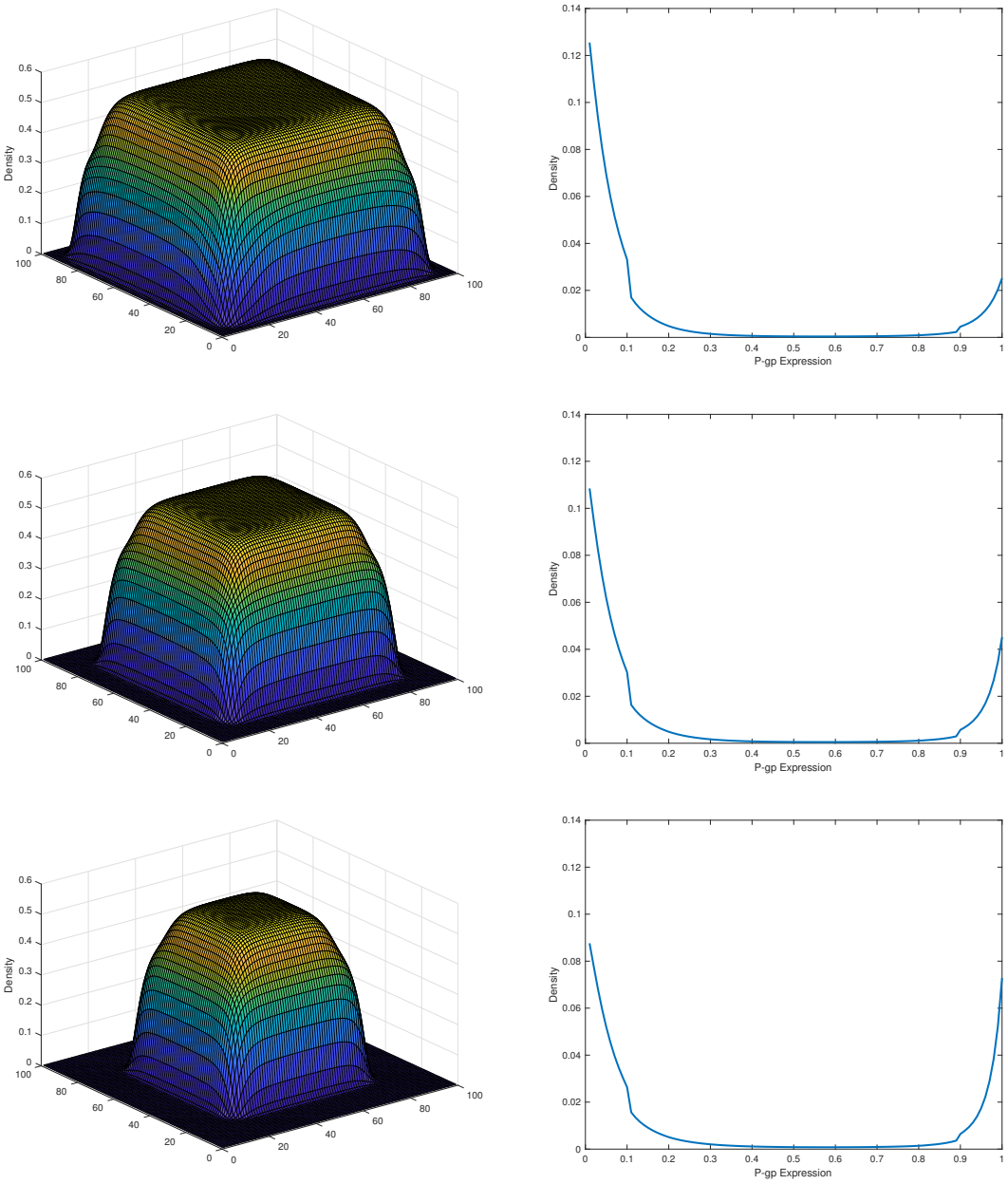

Figure 5.8: Simulation of (5.13) over 100 hours with constant drug doses and high initial values of very resistant and very sensitive cells. Left: Overall tumor density. Right: Density of tumor cells at each level of P-gp expression. Top: c=5. Middle: c=50. Bottom: c=500.

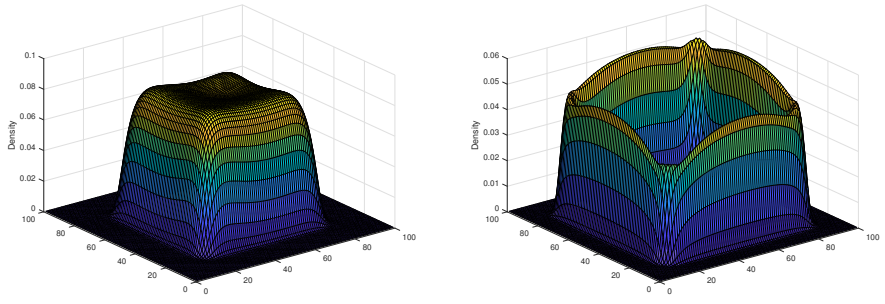

Figure 5.9: Simulation of (5.13) over 100 hours with constant drug dose c=50. Left: Density of tumor cells with resistance level $p = 0.01$. Right: Density of tumor cells with resistance level 0.99.

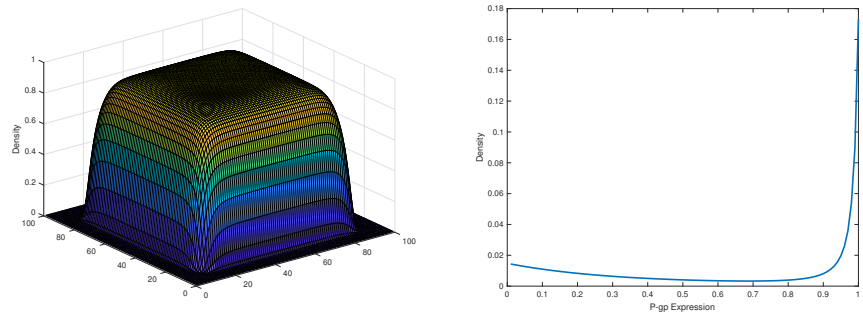

Figure 5.10: Simulation of (5.13) over 100 hours with constant drug dose c=50 and equal initial amounts of every resistance level. Left: Overall tumor density. Right: Density of tumor cells at each level of P-gp expression.

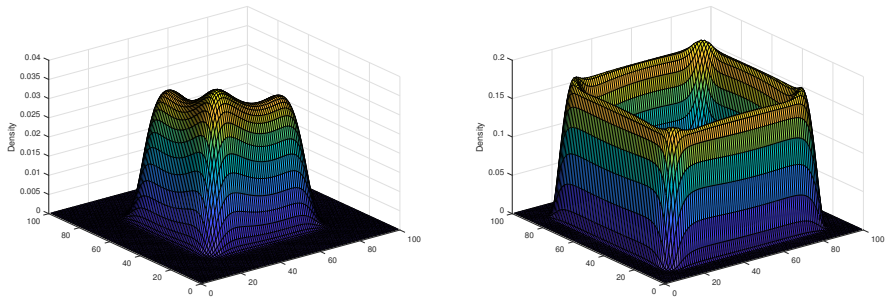

Figure 5.11: Simulation of (5.13) over 100 hours with constant drug dose c=50 and equal initial amounts of every resistance level. Left: Density of tumor cells with resistance level $p = 0.01$. Right: Density of tumor cells with resistance level 0.99.

is still allowing for some growth and that is explained further in Figure 5.11, where we see the distribution of the most sensitive cells in the domain. The drug does not have as much effect in the center of the tumor where the sensitive cells may continue to grow. The most resistant cells cannot compete with the sensitive cells but they grow near the boundary where the most sensitive cells have all been killed by the drug.

We are interested in the most effective therapy for eradicating, or at least controlling, the tumor. In the following section we explore treatment protocols and find the optimal solutions.

5.3.2 Optimal Therapies

As in Section 4.4.3, we study treatment protocols and objectives. Recalling (4.10), we set:

$$J = \int_0^{t_{end}} u^m \, dt. \tag{5.15}$$

Again, $m = 1$ for linear control and $m = 2$ for quadratic control. We state u as $\sum_{i=1}^{N}\sum_{j=1}^{N}\sum_{m=1}^{Nm} u_(i,j,p)$, the total amount of cancer cells in our domain at each time step.

As in Section 4.4.3 we do not need to optimize over every possible drug treatment protocol. Instead, we optimize over the same set of reasonable drug doses and time frames. We allow for constant infusion as well as on/off infusion with 8 hours on delivered every 12 hours as well as every 24, 36, and up to one month. We use Matlab to find not only the minimum J but also what protocol minimizes the tumor size at the end of the simulation, $u(:,:,t_{end})$. In addition, we also use the same process to minimize:

$$J_d = \int_0^{t_{end}} \delta_u u^m + \delta_c c^m \, dt. \tag{5.16}$$

This functional measures not only the overall tumor size but also the total amount of drug. We do not include healthy cells in this study but it is known that large doses of chemotherapy have unwanted negative effects on healthy cells so we want to minimize not only the size of the tumor but also the total amount of drugs administered.

We achieve a similar result as in Section 4.4.3: The best way to control the tumor size under the effects of a cytotoxic drug is either to administer a maximal continuous dose or to administer no drug at all. Administration of no drug allows the more sensitive cells to exhibit a control over the more resistant cells will keep the resistant cells from taking over. If large amounts of the drug are infused then the resistant cells will take over and then the drug is unable to stop the tumor from

growing.

Once again, we showed that in a spatial model exhibiting heterogeneity in P-gp expression levels we cannot achieve a positive result as a function of treatment with a cytotoxic agent alone. Changing from a discrete model of P-gp expression to a continuous variable does not change the final outcome.

5.4 Extension to Two Transfer Rules

We conclude with a brief study of multiple transfer rules. We now incorporate two different types of P-gp transfer (as in [3]). In this case our equation for $u(p, x, t)$ is still (5.5) but we now allow for $f = f_1$ or $f = f_2$. Following [3], we keep the probabilities π_1 and π_2 as defined in (5.4). We now write $\hat{T}(u)(p)$ as:

$$\begin{aligned}\hat{T}(u)(p) \coloneqq &\int \pi_1 u\left(\frac{p - p_2 f_1}{1 - f_1}\right) u(p_2)dp_2 + \int \pi_1 u\left(\frac{p - (1 - f_1)p_2}{f_1}\right) u(p_2)dp_2 \\ &+ \int \pi_2 u\left(\frac{p - p_2 f_2}{1 - f_2}\right) u(p_2)dp_2 + \int \pi_2 u\left(\frac{p - (1 - f_2)p_2}{f_2}\right) u(p_2)dp_2.\end{aligned} \tag{5.17}$$

5.4.1 Simulations of the Two Transfer Rule Model (5.17)

Table 5.3 shows the parameters used in simulations with the new transfer rule (5.17). We set $f_1 = 0.48$ and $f_2 = 0.07$. These parameter values come from [3] and we run simulations with them to see if they result in a qualitative difference in our model.

Figure 5.12 shows the result of our first simulation. We use $a(p) = a$, a

Table 5.3: Parameters values used in simulations of (5.5), (5.6), and (5.17) with two transfer efficiency rates.

Parameter	N_z	N_m	dt	dz	D	D_c	
Value	100	100	1	0.5	0.05	1	
Parameter	τ	f_1	f_2	ϵ_f	ϵ	a	γ
Value	0.9	0.48	0.07	0.01	0.5	0.85	0.4

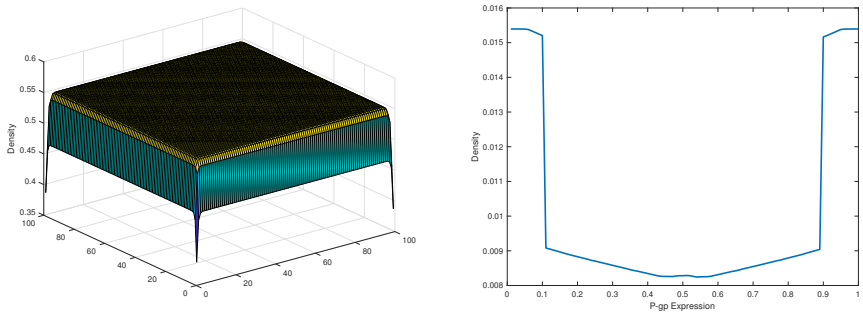

Figure 5.12: Simulation of (5.5), (5.6), and (5.17) over 100 hours with high initial amounts of very sensitive and very resistant cells. Left: Overall tumor density. Right: Density of tumor cells at each level of P-gp expression.

constant. Both figures closely resemble Figure 5.4. There is a slight difference around resistance levels $0.1, 0.5$, and 0.9, but the overall pattern is almost identical. Figure 5.13 shows the same simulation but with $a(p) = 0.85 + 0.15(1 - p)$. Again we see a very similar result to Figure 5.7. It is a smoother curve but the qualitative behavior remains the same.

We conclude that the model with a single transfer rule is sufficient for studying the case of the inclusion of a cytotoxic drug.

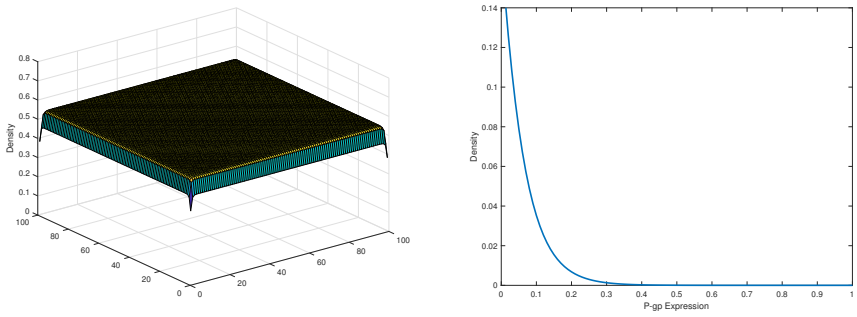

Figure 5.13: Simulation of (5.5), (5.6), and (5.17) over 100 hours with equal initial amounts of every resistance level. Left: Overall tumor density. Right: Density of tumor cells at each level of P-gp expression.

5.5 Discussion

In Chapter 5 we integrated our approach from Chapter 4 with the work of Magal, Pasquier, *et. al* [3, 44]. Using a continuous variable for P-gp expression, we wrote a PDE model with a Boltzmann type integral describing transfer of resistance levels. We simulated and analyzed our output to compare it to the previous results. Without data to optimize parameters we used a combination of already optimized

parameters from Chapter 4 alongside given values for new parameters. We showed that our model can capture the qualitative behavior shown previously. We briefly considered the role of multiple transfer rules. Our simulations showed almost no changes compared with a single rule.

We extended this model to include a cytotoxic drug that acts on the tumor cells through a mass action term. We showed that constant infusion leads to a marked increase in resistant cells, and that a cytotoxic agent alone cannot control the overall tumor growth. Future work will include the addition of combination therapies and a study of their efficacy in controlling (and potentially) eradicating the tumor.

Chapter 6: Conclusion

Cancer is the second leading cause of death in the United States, with over 1.5 million new cases each year [4]. The probability of diagnosis with any invasive cancer is right around 40% [4]. Detection, treatments, and therapies are all continuing to improve and several cancers have high 5-year survival rates when found early enough.

Resistance to anti-cancer drugs continues to be an important obstacle to overcome. There are several genetic factors that lead to drug resistance along with natural selection as drugs are administered. P-glycoprotein is an ABC transporter shown to confer resistance to chemotherapy [40–43]. Its overexpression can lead to resistance levels one hundred times higher than normal tumor cells [46].

Applied mathematicians have not widely studied the transfer of P-gp. The purpose of this dissertation was to research the current mathematical models of P-gp and provide novel ideas to extend this field. In this dissertation we presented three new mathematical models of the transfer of the protein pump P-Glycoprotein and its effect on drug resistance.

Our first model provided an extension of the ODE models of [1]. In [1] the authors wrote an system of ordinary differential equations describing the changes in sensitive tumor cells, resistant tumor cells, and temporarily resistant tumor cells.

They incorporated temporary resistance in their model by allowing sensitive cells to become temporarily resistant after interaction with resistant cells. Those temporarily resistant cells then stay in that phenotype for a prescribed amount of time before they turn back into sensitive cells. This representation is driven by the fact that this high P-gp level is a phenotypic and not genotypic change, thereby meaning that after a few generations the progeny will be back to fully sensitive.

Our approach was to consider a cell-cycle model. We modeled three compartments: quiescent, proliferating, and apoptotic. We allowed cells in the quiescent stage to be either resistant or sensitive and modeled that switch to temporary resistance during the shift from quiescence to proliferative stage. The proliferating cells were broken up into three types: sensitive, resistant, and fully resistant. In keeping with the understanding that those temporarily resistant cells do not keep their resistance for very long, we stated that all progeny of temporarily resistant cells were sensitive. We did not distinguish between the phenotypes in the apoptotic stage. Once cells entered that stage they did not interact with others until dying off and leaving the system completely. We showed that our model provided a better fit for the dynamics of the experimental data in [1].

Our second model incorporated the idea of a discrete representation for P-gp-based drug resistance into a 2-dimensional spatial domain. We again extended the work of [1] but this time into space rather than the cell cycle. We started with a reaction diffusion system of two equations, one for sensitive cells $u(x,t)$, and one for resistant cells $v(x,t)$. The density-inhibited proliferation allowed us to show that the addition of the two equations led to a single Fisher-KPP equation with steady

states at 0 and at full carrying capacity. In this case the tumor continued growing toward the stable carrying capacity steady state.

We extended this approach with the addition of a temporarily resistant phenotype. We used this model to study the experimental data of [1]. We optimized parameters and showed an improved fit to the experimental data compared with our first model. Separately we added a cytotoxic drug to the model with only sensitive and resistant cells. We showed that a constant drug infusion led to an almost fully resistant tumor. We completed Chapter 4 by tying the two ideas together and writing a PDE system with four equations for sensitive cells, resistant cells, temporarily resistant cells, and the drug. We then studied protocols of constant drug infusion and on/off treatment protocols. We saught an optimal therapy and discovered that the treatment protocol that minimizes the overall tumor size is a constant infusion of a maximal drug dosage. This, however, led to a small tumor dominated by resistant cancer cells. The treatment protocol that minimizes resistant cells was to not treat the tumor at all, letting the sensitive cells control the resistant cell population. With these results we have demonstrated that there is no optimal treatment that can control the growth of the tumor while also controlling the resistant phenotype.

Our final model extended the integro-differential equation of Magal *et. al* [3], in which tumor cells $u(x,t)$ were assumed to have a continuous variable x describing P-gp expression. The model included a Boltzmann type integral term describing the transfer of P-gp between two cells. The integral contains two transfer rules, describing two different efficiencies of transfer. In each transfer the cell with higher resistance level transfers to the cell with lower resistance a portion that is a function

of the difference in resistance levels.

We extended it by incorporating density-inhibited proliferation along with the inclusion of a two dimensional spatial domain. We wrote our model as a single partial differential equation with resistance variable p, 2-dimensional space variable x, and time t. We first showed that our model is consistent with the results of [3] in showing that the transfer of resistance leads to equal tumor cell density at each level of resistance. We then incorporated a cytotoxic drug and studied its effects on tumor heterogeneity. Under the assumption that more sensitive cells grow slightly faster we saw that when no drug is present there is a supermajority of sensitive cells. Once the drug is administered, however, the most resistant cells began to grow and dominate. The makeup of the tumor changes, with the most sensitive cells in the center surrounded by very resistant cells. We searched for optimal therapies and, just as in our second model, we were able to show that there is no therapy that will eradicate, or even control, the tumor growth when such resistant cells are present.

Continued work would first rely on access to more experimental data. We were limited in our approaches by the lack of available data concerning P-gp and its transfer between cells. In our cell cycle model we have not yet included any type of drug, and our two PDE models only include a cytotoxic drug. Moving forward could include combination therapies, with the inclusion of immunotherapy and cytostatic drugs.

This work integrated mathematics and cancer biology. Mathematical oncology is an exciting field continuing to grow and the work of mathematicians has been invaluable to the medical community. The future discoveries and models by

mathematicians will continue to be on the frontier of the fight to eradicate cancer.

Bibliography

[1] María Rosa Durán, Ana Podolski-Renić, Arturo Álvarez-Arenas, Jelena Dinić, Juan Belmonte-Beitia, Milica Pešić, and Víctor M Pérez-García. Transfer of drug resistance characteristics between cancer cell subpopulations: A study using simple mathematical models. *Bulletin of mathematical biology*, 78(6):1218–1237, 2016.

[2] James M Greene, Doron Levy, King Leung Fung, Paloma S Souza, Michael M Gottesman, and Orit Lavi. Modeling intrinsic heterogeneity and growth of cancer cells. *Journal of theoretical biology*, 367:262–277, 2015.

[3] P Magal, A Noussair, J Pasquier, P Zongo, and F Le Foll. A model for transfer of p-glycoproteins in mcf-7 breast cancer cell line with multiple transfer rules. *Bulletin of Mathematical Biology*, pages 1–19, 2017.

[4] Rebecca L Siegel, Kimberly D Miller, and Ahmedin Jemal. Cancer statistics, 2016. *CA: a cancer journal for clinicians*, 66(1):7–30, 2016.

[5] Lauren Sompayrac. *How cancer works*. Jones & Bartlett Learning, 2004.

[6] Jonathan Lopez and SWG Tait. Mitochondrial apoptosis: killing cancer using the enemy within. *British journal of cancer*, 112(6):957–962, 2015.

[7] Anthony Letai. Apoptosis and cancer. *Annual Review of Cancer Biology*, 1:275–294, 2017.

[8] Robert Weinberg. *The biology of cancer*. Garland science, 2013.

[9] Eric R Fearon and Bert Vogelstein. A genetic model for colorectal tumorigenesis. *Cell*, 61(5):759–767, 1990.

[10] Richard Doll and Richard Peto. The causes of cancer: quantitative estimates of avoidable risks of cancer in the united states today. *JNCI: Journal of the National Cancer Institute*, 66(6):1192–1308, 1981.

[11] Richard W Clapp, Molly M Jacobs, and Edward L Loechler. Environmental and occupational causes of cancer: new evidence 2005-2007. *Reviews on environmental health*, 23(1):1–38, 2008.

[12] Jiro Inagaki, Victorio Rodriguez, and Gerald P Bodey. Causes of death in cancer patients. *Cancer*, 33(2):568–573, 1974.

[13] American Society of Clinical Oncologists. *Breast Cancer: Statistics*, 2017.

[14] Trachette L Jackson and Helen M Byrne. A mathematical model to study the effects of drug resistance and vasculature on the response of solid tumors to chemotherapy. *Mathematical biosciences*, 164(1):17–38, 2000.

[15] Michael B Sporn. The war on cancer. *The lancet*, 347(9012):1377–1381, 1996.

[16] Siddhartha Mukherjee. The emperor of all maladies. *A biography of cancer. New York: Scribner*, 2010.

[17] Brigid K Killelea, Vicky Q Yang, Sarah Mougalian, Nina R Horowitz, Lajos Pusztai, Anees B Chagpar, and Donald R Lannin. Neoadjuvant chemotherapy for breast cancer increases the rate of breast conservation: results from the national cancer database. *Journal of the American College of Surgeons*, 220(6):1063–1069, 2015.

[18] Pippa G Corrie. Cytotoxic chemotherapy: clinical aspects. *Medicine*, 36(1):24–28, 2008.

[19] Vincent T DeVita and Edward Chu. A history of cancer chemotherapy. *Cancer research*, 68(21):8643–8653, 2008.

[20] Vikas Malhotra and Michael C Perry. Classical chemotherapy: mechanisms, toxicities and the therapeutc window. *Cancer biology & therapy*, 2(sup1):1–3, 2003.

[21] Mohamed Bentires-Alj, Veronique Barbu, Marianne Fillet, Alain Chariot, Biserka Relic, Nathalie Jacobs, Jacques Gielen, Marie-Paule Merville, and Vincent Bours. Nf-κb transcription factor induces drug resistance through mdr1 expression in cancer cells. *Oncogene*, 22(1):90, 2003.

[22] C Keith Bomford, J Miller, H Kunkler, IH Sherriff, SBCK Bomford, SB IH Kunkler, et al. *Walter and Miller's textbook of radiotherapy: radiation physics, therapy, and oncology*. Number Sirsi) i9780443028731. 1993.

[23] Kevin A Camphausen and RC Lawrence. Principles of radiation therapy. *Cancer management: a multidisciplinary approach*, 11:221–230, 2008.

[24] Nicholas L Syn, Michele WL Teng, Tony SK Mok, and Ross A Soo. De-novo and acquired resistance to immune checkpoint targeting. *The Lancet Oncology*, 18(12):e731–e741, 2017.

[25] Lauren M Sompayrac. *How the immune system works*. John Wiley & Sons, 2015.

[26] Ira Mellman, George Coukos, and Glenn Dranoff. Cancer immunotherapy comes of age. *Nature*, 480(7378):480, 2011.

[27] Vishol Chadha and Shrutakirthi D Shenoi. Hair loss in cancer chemotherapeutic patients. *Indian Journal of Dermatology, Venereology, and Leprology*, 69(2):131, 2003.

[28] Genevieve Housman, Shannon Byler, Sarah Heerboth, Karolina Lapinska, Mckenna Longacre, Nicole Snyder, and Sibaji Sarkar. Drug resistance in cancer: an overview. *Cancers*, 6(3):1769–1792, 2014.

[29] Larry Norton and Richard Simon. Tumor size, sensitivity to therapy, and design of treatment schedules. *Cancer treatment reports*, 61(7):1307, 1977.

[30] Richard Simon and Larry Norton. The norton-simon hypothesis: designing more effective and less toxic chemotherapeutic regimens. *Nature Reviews. Clinical Oncology*, 3(8):406, 2006.

[31] Jean-Pierre Gillet and Michael M Gottesman. Mechanisms of multidrug resistance in cancer. *Multi-drug resistance in cancer*, pages 47–76, 2010.

[32] Salvador E Luria and Max Delbrück. Mutations of bacteria from virus sensitivity to virus resistance. *Genetics*, 28(6):491, 1943.

[33] Frédérique Billy, Jean Clairambault, and Olivier Fercoq. Optimisation of cancer drug treatments using cell population dynamics. In *Mathematical Methods and Models in Biomedicine*, pages 265–309. Springer, 2013.

[34] American Cancer Society. *Cancer Facts & Figures*, 2016.

[35] M Cooper Geoffrey, EH Robert, et al. The cell: a molecular approach. *Boston University, Sunderland*, 2000.

[36] Valentina Fodale, Mariaelena Pierobon, Lance Liotta, and Emanuel Petricoin. Mechanism of cell adaptation: when and how do cancer cells develop chemoresistance? *The Cancer Journal*, 17(2):89–95, 2011.

[37] Amy L Davidson, Elie Dassa, Cedric Orelle, and Jue Chen. Structure, function, and evolution of bacterial atp-binding cassette systems. *Microbiology and Molecular Biology Reviews*, 72(2):317–364, 2008.

[38] Gregory D Leonard, Tito Fojo, and Susan E Bates. The role of abc transporters in clinical practice. *The oncologist*, 8(5):411–424, 2003.

[39] K Ueda, DP Clark, CJ Chen, IB Roninson, MM Gottesman, and I Pastan. The human multidrug resistance (mdr1) gene. cdna cloning and transcription initiation. *Journal of Biological Chemistry*, 262(2):505–508, 1987.

[40] Piet Borst, Raymond Evers, Marcel Kool, and Jan Wijnholds. A family of drug transporters: the multidrug resistance-associated proteins. *Journal of the National Cancer Institute*, 92(16):1295–1302, 2000.

[41] C Cordon-Cardo, JP O'Brien, J Boccia, D Casals, JR Bertino, and MR Melamed. Expression of the multidrug resistance gene product (p-glycoprotein) in human normal and tumor tissues. *Journal of Histochemistry & Cytochemistry*, 38(9):1277–1287, 1990.

[42] James M Ford, Jin-Ming Yang, and William N Hait. P-glycoprotein-mediated multidrug resistance: experimental and clinical strategies for its reversal. In *Drug Resistance*, pages 3–38. Springer, 1996.

[43] PF Juranka, RL Zastawny, and V Ling. P-glycoprotein: multidrug-resistance and a superfamily of membrane-associated transport proteins. *The FASEB Journal*, 3(14):2583–2592, 1989.

[44] Jennifer Pasquier, Ludovic Galas, Céline Boulangé-Lecomte, Damien Rioult, Florence Bultelle, Pierre Magal, Glenn Webb, and Frank Le Foll. Different modalities of intercellular membrane exchanges mediate cell-to-cell p-glycoprotein transfers in mcf-7 breast cancer cells. *Journal of Biological Chemistry*, 287(10):7374–7387, 2012.

[45] Franz Thiebaut, Takashi Tsuruo, Hirofumi Hamada, Michael M Gottesman, Ira Pastan, and Mark C Willingham. Cellular localization of the multidrug-resistance gene product p-glycoprotein in normal human tissues. *Proceedings of the National Academy of Sciences*, 84(21):7735–7738, 1987.

[46] Albert Breier, Lenka Gibalova, Mario Seres, Miroslav Barancik, and Zdenka Sulova. New insight into p-glycoprotein as a drug target. *Anti-Cancer Agents in Medicinal Chemistry (Formerly Current Medicinal Chemistry-Anti-Cancer Agents)*, 13(1):159–170, 2013.

[47] Suresh V Ambudkar, Zuben E Sauna, Michael M Gottesman, and Gergely Szakacs. A novel way to spread drug resistance in tumor cells: functional intercellular transfer of p-glycoprotein (abcb1). *Trends in pharmacological sciences*, 26(8):385–387, 2005.

[48] Andre Levchenko, Bipin M Mehta, Xinle Niu, Grace Kang, Liliana Villafania, Denise Way, Dolores Polycarpe, Michel Sadelain, and Steven M Larson. Intercellular transfer of p-glycoprotein mediates acquired multidrug resistance in tumor cells. *Proceedings of the National Academy of Sciences of the United States of America*, 102(6):1933–1938, 2005.

[49] Jennifer Pasquier, Pierre Magal, Céline Boulangé-Lecomte, Glenn Webb, and Frank Le Foll. Consequences of cell-to-cell p-glycoprotein transfer on acquired multidrug resistance in breast cancer: a cell population dynamics model. *Biology direct*, 6(1):1, 2011.

[50] AJ Coldman and JH Goldie. Role of mathematical modeling in protocol formulation in cancer chemotherapy. *Cancer treatment reports*, 69(10):1041–1048, 1985.

[51] R Rosen. " role of mathematical modeling in protocol formulation in cancer chemotherapy". *Cancer treatment reports*, 70(12):1461–1462, 1986.

[52] Brian G Birkhead, Elaine M Rankin, Stephen Gallivan, Leanne Dones, and Robert D Rubens. A mathematical model of the development of drug resistant to cancer chemotherapy. *European Journal of Cancer and Clinical Oncology*, 23(9):1421–1427, 1987.

[53] BG Birkhead and WM Gregory. A mathematical model of the effects of drug resistance in cancer chemotherapy. *Mathematical biosciences*, 72(1):59–69, 1984.

[54] WM Gregory, BG Birkhead, and RL Souhami. A mathematical model of drug resistance applied to treatment for small-cell lung cancer. *Journal of Clinical Oncology*, 6(3):457–461, 1988.

[55] RL Souhami, WM Gregory, and BG Birkhead. Mathematical models in high-dose chemotherapy. In *Treatment Modalities in Lung Cancer*, volume 41, pages 21–28. Karger Publishers, 1988.

[56] John Carl Panetta. A mathematical model of drug resistance: heterogeneous tumors. *Mathematical biosciences*, 147(1):41–61, 1998.

[57] Orit Lavi, James M Greene, Doron Levy, and Michael M Gottesman. The role of cell density and intratumoral heterogeneity in multidrug resistance. *Cancer research*, 73(24):7168–7175, 2013.

[58] Orit Lavi, Michael M Gottesman, and Doron Levy. The dynamics of drug resistance: a mathematical perspective. *Drug Resistance Updates*, 15(1):90–97, 2012.

[59] Alexander Lorz, Tommaso Lorenzi, Michael E Hochberg, Jean Clairambault, and Benoît Perthame. Populational adaptive evolution, chemotherapeutic resistance and multiple anti-cancer therapies. *ESAIM: Mathematical Modelling and Numerical Analysis*, 47(2):377–399, 2013.

[60] AJ Coldman and JH Goldie. A model for the resistance of tumor cells to cancer chemotherapeutic agents. *Mathematical Biosciences*, 65(2):291–307, 1983.

[61] Alexander Lorz, Tommaso Lorenzi, Jean Clairambault, Alexandre Escargueil, and Benoît Perthame. Modeling the effects of space structure and combination therapies on phenotypic heterogeneity and drug resistance in solid tumors. *Bulletin of mathematical biology*, 77(1):1–22, 2015.

[62] Lisette G De Pillis and Ami Radunskaya. A mathematical tumor model with immune resistance and drug therapy: an optimal control approach. *Computational and Mathematical Methods in Medicine*, 3(2):79–100, 2001.

[63] Lisette G De Pillis and A Radunskaya. The dynamics of an optimally controlled tumor model: A case study. *Mathematical and computer modelling*, 37(11):1221–1244, 2003.

[64] Lisette G de Pillis, Weiqing Gu, and Ami E Radunskaya. Mixed immunotherapy and chemotherapy of tumors: modeling, applications and biological interpretations. *Journal of theoretical biology*, 238(4):841–862, 2006.

[65] Urszula Ledzewicz and Heinz M Schättler. Drug resistance in cancer chemotherapy as an optimal control problem. *Discrete and Continuous Dynamical Systems Series B*, 6(1):129, 2006.

[66] Lev Semenovich Pontryagin. *Mathematical theory of optimal processes*. CRC Press, 1987.

[67] Heinz Schättler and Urszula Ledzewicz. *Geometric optimal control: theory, methods and examples*, volume 38. Springer Science & Business Media, 2012.

[68] Heinz Schättler and Urszula Ledzewicz. *Optimal control for mathematical models of cancer therapies*. Springer, 2015.

[69] Seth Michelson and Doris Slate. A mathematical model of the p-glycoprotein pump as a mediator of multidrug resistance. *Bulletin of mathematical biology*, 54(6):1023–1038, 1992.

[70] Seth Michelson and Doris Slate. A mathematical model for the inhibition of the multidrug resistance-associated p-glycoprotein pump. *Bulletin of mathematical biology*, 56(2):207–223, 1994.

[71] Vasiliki Panagiotopoulou, Giles Richardson, Oliver E Jensen, and Cyril Rauch. On a biophysical and mathematical model of pgp-mediated multidrug resistance: understanding the ?space–time? dimension of mdr. *European Biophysics Journal*, 39(2):201, 2010.

[72] Leonora Balaj, Ryan Lessard, Lixin Dai, Yoon-Jae Cho, Scott L Pomeroy, Xandra O Breakefield, and Johan Skog. Tumour microvesicles contain retrotransposon elements and amplified oncogene sequences. *Nature communications*, 2:180, 2011.

[73] Matthew Becker and Doron Levy. Modeling the transfer of drug resistance in solid tumors. *Bulletin of mathematical biology*, 79(10):2394–2412, 2017.

[74] Kyle R Brimacombe, Matthew D Hall, Douglas S Auld, James Inglese, Christopher P Austin, Michael M Gottesman, and King-Leung Fung. A dual-fluorescence high-throughput cell line system for probing multidrug resistance. *Assay and drug development technologies*, 7(3):233–249, 2009.

[75] Péter Hantz. Pattern formation in a new class of precipitation reactions. *Doctorate of Sciences thesis (Physics), University of Geneva, Geneva*, 2006.

[76] Alan Mathison Turing. The chemical basis of morphogenesis. *Philosophical Transactions of the Royal Society of London. Series B, Biological Sciences*, 237(641):37–72, 1952.

[77] CV Pao. Global asymptotic stability of lotka–volterra competition systems with diffusion and time delays. *Nonlinear Analysis: Real World Applications*, 5(1):91–104, 2004.

[78] Ronald Aylmer Fisher. The wave of advance of advantageous genes. *Annals of Human Genetics*, 7(4):355–369, 1937.

[79] AN Kolmogorov, IG Petrovsky, and NS Piskunov. Investigation of a diffusion equation connected to the growth of materials, and application to a problem in biology. *Bull. Univ. Moscow, Ser. Int. Sec. A*, 1(1), 1937.

[80] Peter Hinow, Frank Le Foll, Pierre Magal, and Glenn F Webb. Analysis of a model for transfer phenomena in biological populations. *SIAM Journal on Applied Mathematics*, 70(1):40–62, 2009.